

Big Bang Nucleosynthesis Constraints on Hadronically and Electromagnetically Decaying Relic Particles

Karsten Jedamzik

Laboratoire de Physique Mathématique et Théorique,
Université de Montpellier II, 34095 Montpellier Cedex 5, France

Big Bang nucleosynthesis in the presence of decaying relic particles is examined in detail. All non-thermal processes are important for the determination of light-element abundance yields of ^2H , ^3H , ^3He , ^4He , ^6Li , and ^7Li are coupled to the thermal nuclear fusion reactions to obtain comparatively accurate results. Predicted light-element yields are compared to observationally inferred limits on primordial light-element abundances to infer constraints on the abundances and properties of relic decaying particles with decay times in the interval $0.01 \text{ sec} < \tau_x < 10^{12} \text{ sec}$. Decaying particles are typically constrained at early times by ^4He or ^2H , at intermediate times by ^6Li , and at large times by the $^3\text{He}/^2\text{H}$ ratio. Constraints are shown for a large number of hadronic branching ratios and decaying particle masses and may be applied to constrain the evolution of the early Universe.

PACS numbers:

I. INTRODUCTION

The epoch of Big Bang nucleosynthesis (BBN) is one of the furthest reaching back probe of early cosmological conditions. It has thus been invaluable, for example, for the realization that baryonic matter contributes only a small fraction to the present critical density, thus providing independent evidence for the existence of dark matter, or that extensions of the standard model of particle physics which include further light degrees of freedom are observationally disfavored. Due to its usefulness BBN has thus been analysed in many variants (inhomogeneous BBN, BBN with leptonic chemical potentials, BBN with antimatter domains, BBN with decaying particles or evaporating primordial black holes, BBN with Brans-Dicke gravity, etc. – for reviews the reader is referred to Ref. [1]). These studies have been important for the realization that the Universe must have been fairly close during the BBN epoch ($1-10^4 \text{ sec}$) to that described by the standard model of BBN (SBBN). An SBBN scenario assumes a homogeneous baryonic plasma free of defects or decaying relics and with close-to-vanishing leptonic chemical potentials at constant baryon-to-entropy. With the recent accurate determination of the fractional contribution of baryons to the critical density $bh^2 = 0.0223^{+0.0007}_{-0.0009}$ (h is the Hubble constant in units $100 \text{ km s}^{-1}\text{Mpc}^{-1}$) by the WMAP satellite mission [2] predicted primordial light-elements in a SBBN scenario may be compared with those observationally inferred. This comparison is good when $^2\text{H}/\text{H}$ is considered, fair when ^4He , and inconclusive when ^3He is considered, but factor 2–3 discrepant in the case of ^7Li . It is not clear if this latter discrepancy is due to stellar ^7Li destruction effects, either in Pop II [3, 4, 5] stars where it is observed, or in a prior Pop III generation [7], or indeed due to a required modification of BBN, such as a population of decaying relics [8, 9]. This discrepancy, however, is not subject of the present paper.

The current study presents in detail analysis and results of BBN with decaying particles. Such scenarios may easily emerge, for example, in supersymmetric extensions of the standard model, where relic gravitinos produced at high temperatures decay during BBN [10]. Similarly, when the gravitino is the lightest supersymmetric particle, next-to-lightest supersymmetric states or binos may decay into gravitinos during or after BBN. Many such BBN studies have been presented before, from the pioneering works in the eighties [11, 12, 13, 14, 15] to improved and updated analysis in the nineties [16, 17, 18] up to very recent publications [8, 19, 20, 21]. Nevertheless, except for Ref. [8, 20, 21] none of these works were able to properly treat the hadronic decay of a relic particle during BBN.

The purpose of this paper is twofold. It is intended to present a catalog of constraints on hadronically and electromagnetically decaying particles over a wide range of decay times ($10^{-2}-10^{12} \text{ sec}$) as well as hadronic branching ratios and relic particle masses. Prior studies have presented results only for a very small number of hadronic branching ratios. It should be noted that due to nonlinearities, either at smaller decay times ($< 10^4 \text{ sec}$) when thermal nuclear reactions still proceed or due to interference of electromagnetic destruction and hadronic production, for example, a simple interpolation between results at different hadronic branching ratios often leads to erroneous or inaccurate results. The second purpose of this study is to present the detailed analysis underlying the results presented in Ref. [8, 9, 22, 23]. In general the philosophy in the analysis is to stay as close as possible to experimental data. Furthermore, a large number (93, cf. Table I) of processes are included, all those which the author believes to play a role at the more than a few per cent level. Particular attention is given to an as accurate as possible determination

of the synthesized ^6Li in such scenarios. This is also of importance as ^6Li has been recently observed in surprisingly large abundance in about 10 Pop II stars [24] and is often a byproduct of decaying [14, 17] or annihilating [22] relic particles.

The outline of the paper is as follows. In Sec. II a brief overview over the physics of BBN in the presence of electromagnetically and hadronically decaying particles is presented. Sec. III discusses observationally inferred primordial light-element abundances and derives the constraints on those as applied in the analysis. Sec. IV then presents the constraints which apply to the abundance of putative relic decaying particles, whereas conclusions are drawn in Sec. V. For the interested reader and for the benefit of the author, a number of appendices summarizes the analysis. This includes general considerations (App. A), the numerical procedure (App. B), employed kinematic relations (App. C), non-thermal electromagnetic interactions (App. D), non-thermal hadronic interactions (App. E), and the thermal nuclear reactions (App. F).

II. OVERVIEW OF THE PHYSICS OF BBN WITH DECAYING PARTICLES

This section gives a brief and schematic account of the modifications to BBN when energetic particles are injected due to, for example, the decay of relic particles. The decay channel of the relic determines the energy and nature of the injected primaries. A BBN calculation with decaying particles requires the detailed study of the thermalization of these primaries in the primordial plasma, as well as that of secondaries produced during the thermalization process. Since for one energetic primary several tens/hundreds of secondaries may be produced such calculations are sometimes also referred to as cascade nucleosynthesis calculations. In addition, thermal nuclear reactions operative at early times ($< 10^4$ sec) have to be followed. One distinguishes between primaries being either hadronic (nucleons, antinucleons, mesons), electromagnetic (photons, e^\pm), or inert (neutrinos or other weakly interacting particles). This distinction is useful as the thermalization of hadronically and electromagnetically interacting particles is very different and thus impacts the light-element yields in different ways. Both have nevertheless in common that over the whole range of decay times considered here (10^2 – 10^{12} sec) thermalization occurs very rapidly on the Hubble scale. Redshifting of energetic particles has therefore not to be considered. In contrast, inert particles, such as neutrinos have typically no further interactions with the plasma and thus also do not affect BBN yields. However, even neutrinos, if energetic enough (> 100 GeV) and injected very early on (< 1 sec) may not be regarded as inert (cf. App. E 1), but since their effects are typically subdominant compared to hadronically and electromagnetically interacting particles, they are not considered in the present study.

Hadronically interacting primaries may affect light-element yields in the whole above quoted decay time range. Charged mesons have an effect only during early times ($< 10^1$ – 10^2 sec) due to charge exchange reactions [15] (Rec. 34–43 Table I, App. E 1) with nucleons, converting mostly protons to neutrons and thereby increasing the ^4He abundance. At larger decay times their effects are negligible since they mostly decay before reacting with nucleons. At shorter decay times thermal weak interactions very quickly re-establish the SBBN neutron-to-proton ratio. Antinucleons may have an effect at all times, though their effect is the most pronounced during the time interval 10^1 – 10^2 sec (App. E 2). As they are more likely to annihilate on protons they also tend to increase the neutron-to-proton ratio. At times > 200 sec a significant fraction $Y_p = 0.25$ of all baryons are bound into helium nuclei. Annihilation of antinucleons on helium nuclei may leave ^2H , ^3H , and ^3He as secondaries [11]. However, this effect is subdominant as compared to the effects by injected nucleons.

Neutrons at > 200 sec and protons at $> 10^4$ sec thermalize to a substantial degree via nucleon-nucleon collisions (Rec. 48–73 Table I, App. E 3, E 4) and nuclear spallation reactions (Rec. 74–83 Table I, App. E 5). This is because the competing processes for thermalization, magnetic moment scattering of neutrons off plasma and (Rec. 3, App. D 1.c), Coulomb stopping of protons by plasma (Rec. 1, App. D 1.a), and Thomson scattering of protons on CMBR photons (Rec. 2, App. D 1.b) lose their efficiency. This holds true except for very energetic nucleons as well as protons in the tens of MeV range and is due to ever decreasing numbers of and energy of CMBR photons. These results may be observed in Fig. 1. Each nucleon-nucleon scattering produces another energetic nucleon. The injection of an energetic 100 GeV nucleon may therefore lead to the production of several tens of 1 GeV nucleons. Their collective impact on the light-element yields via spallation of ^4He to produce ^2H , ^3H , and ^3He , is far greater than that of a 100 GeV injected antinucleon [14]. The latter undergoes maximal 2–3 scattering before annihilating, with the respective probability of spallation of ^4He being comparably small. The injection of nucleons is therefore always important. At early times this is due to an increase of the neutron density (< 1 – 10 sec) leading to either an increased ^4He (< 200 sec), increased ^2H (< 200 – 10^2 sec), or decreased ^7Li ($< 10^3$ sec) abundance. Somewhat later, and for the whole range of decay times considered here (> 200 sec) spallation of ^4He by energetic nucleons and their secondaries yields large amounts of ^2H , ^3H , and ^3He . These trends may be seen in Fig. 3. As ^4He spallation

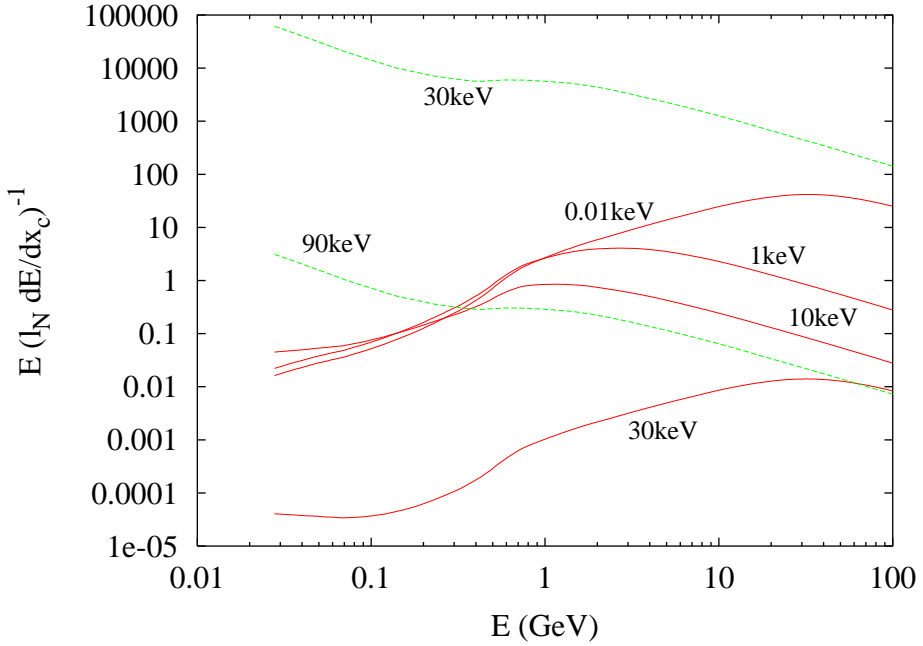


FIG. 1: The quantity $E (l_N dE/dx_C)^{-1}$ as a function of nucleon energy E , where l_N is the nucleon mean free path and dE/dx_C is the nucleon energy loss per unit path length due to 'continuous' energy losses such as multiple Coulomb scattering. When $E (l_N dE/dx_C)^{-1} > 1$ nucleons predominantly lose energy due to nucleon-nucleon scattering and spallation processes, whereas in the opposite case nucleons lose their energy predominantly continuously via multiple electromagnetic scatterings on electrons and photons (cf. Eq. B.1). Only in the former limit nuclear cascades occur. The quantity is shown for neutrons (green - dashed) at temperatures $T = 90$ and 30 keV and protons (red - solid) at temperatures $T = 30; 10; 1$ and 0.01 keV as labeled in the figure.

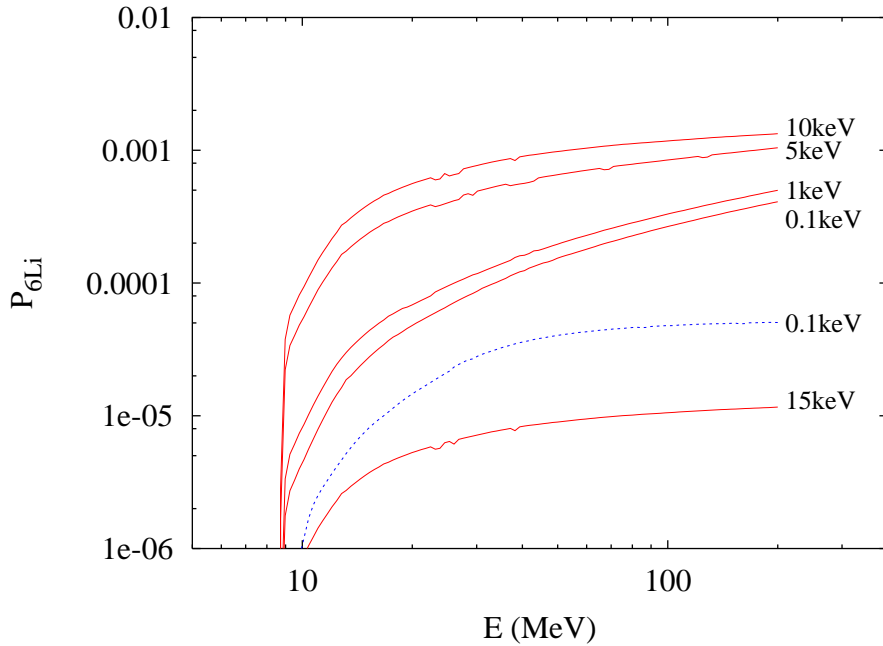


FIG. 2: Probability P_{6Li} of energetic 3H nuclei (red - solid) and energetic 3He (blue - dotted) of initial energy E to fuse on ambient 4He nuclei to form 6Li via the reactions $^3H(n, p) ^6Li$ and $^3He(p, n) ^6Li$, respectively. The figure shows this probability for 3H -nuclei at temperatures $T = 5; 10; 5; 1$ and 0.1 keV and for 3He -nuclei at temperature $T = 0.1$ keV, respectively. Survival of the freshly formed 6Li -nuclei against thermal nuclear reactions is also taken into account as evident by the comparatively low P_{6Li} at $T = 15$ keV. The figure illustrates that P_{6Li} dramatically increases at $T = 5 - 10$ keV due to a decrease of the efficiency of Coulomb stopping in this narrow temperature interval (see text).

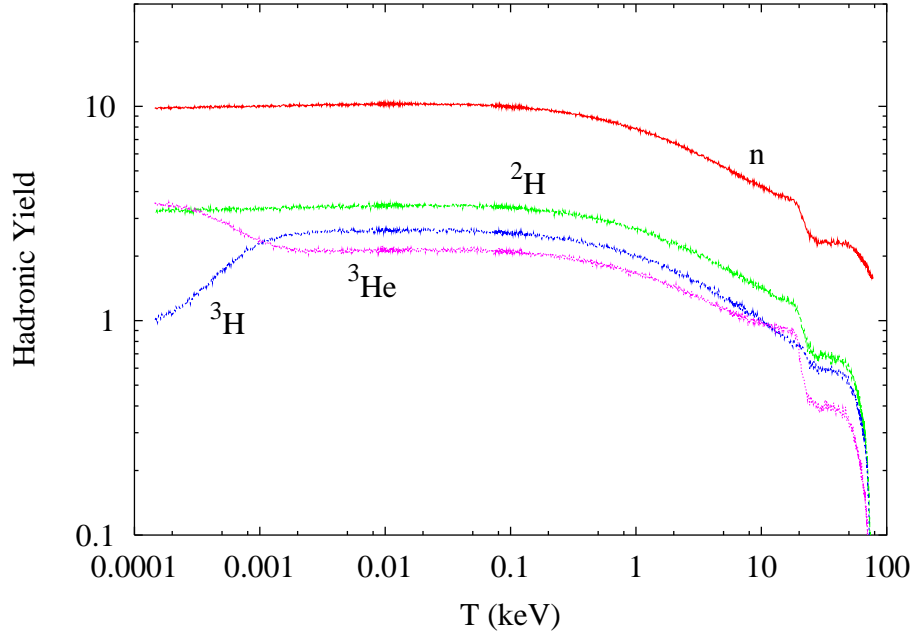


FIG. 3: Yields of (from top to bottom) neutrons (red), deuterium nuclei (green), tritium nuclei (blue), and ^3He -nuclei (magenta) as a function of cosmic temperature T per hadronically decaying particle X^- ! $q\bar{q}$ of mass $M_x = 1\text{ TeV}$, where q denotes a quark. Note that initially after hadronization of the $q\bar{q}$ state on average only 1.56 neutrons result. The remainder of the created neutrons at lower temperatures $T < 90\text{ keV}$ are resulting from the thermalization of the injected neutrons (and protons) due to inelastic nucleon-nucleon scattering processes and ^4He spallation processes. Similarly, all the ^2H , ^3H , and ^3He nuclei are due to ^4He spallation processes and np nonthermal fusion reactions (for ^2H) induced by the thermalization of the injected energetic nucleons. The figure does not include the electromagnetic yields (cf. Fig. 4) due to photodisintegration which is inevitable even for a hadronic decay since approximately 45% of the rest mass energy of the decaying particle is converted into energetic γ -rays and energetic e^- after hadronization and pion decays.

processes by neutrons in the time range $200 - 10^6\text{ sec}$ are by far more efficient than those by protons, inelastic nucleon-nucleon reactions (Rec. 52-73, App. E.4) which preferentially convert protons to neutrons are also important for accurate BBN yield predictions.

The spallation of ^4He to form ^3H and ^3He is also important as it may lead to the synthesis of ^6Li [14] (cf. App. E.6). The mass three nuclei ^3H and ^3He emerge energetic from these reactions with typical energies around 10 MeV . They may thus participate in the non-thermal fusion reactions 85-86 to form ^6Li . The formation of ^7Li by those energetic 3-nuclei, as well as by energetic ^4He resulting from elastic nucleon- ^4He collisions (Rec. 87-88) is by far less important. Energetic mass three nuclei to the largest part lose their energy efficiently via Coulomb stopping. However, even the comparatively small fraction $\sim 10^{-4}$ (cf. Fig. 2) which fuses may yield an observationally important ^6Li abundances. The freshly fused ^6Li may survive thermal nuclear reactions only above $> 10^4\text{ sec}$. A particularity in the Coulomb stopping (cf. App. D.1.a) which renders it very much less efficient for nuclei with velocities below the thermal electron velocity, which is the case for $< 10\text{ MeV}$ 3-nuclei at $< 10^6\text{ sec}$ increases the ^6Li production efficiency around this time by a factor of ten. As explained in App. E.6 ^6Li yields due to energetic mass three nuclei produced by ^4He spallation are somewhat uncertain and may well be some tens of per cents higher. The uncertainty is due to an incomplete knowledge of the high-energy tail of produced mass three nuclei which may well include a backward scattering peak. The present study is therefore conservative in estimating ^6Li yields.

Electromagnetically interacting particles may impact BBN yields only at comparatively large decay times ($> 10^5\text{ sec}$). This is due to energetic photons and e^- interacting efficiently with CMBR photons (cf. App. D.2). γ -rays rapidly pair-produce on CMBR photons (Rec. 4) and electrons inverse Compton scatter (Rec. 5). Comparatively long-lived against further interactions are only γ -rays of energies below the e^- pair production threshold. This threshold is at $E = 2.2\text{ MeV}$ at $< 10^6\text{ sec}$ and increases continuously as the CMBR temperature drops reaching $E = 19.8\text{ MeV}$ at

$< 10^7\text{ sec}$. These latter energies are the thresholds for photodisintegration of ^2H and ^4He , respectively. Once γ -rays have dropped below the pair production threshold their interactions close to the threshold are dominated by scattering of CMBR photons (App. E.2.d), and further below the threshold by either-Heitler pair production (App. E.2.a) and

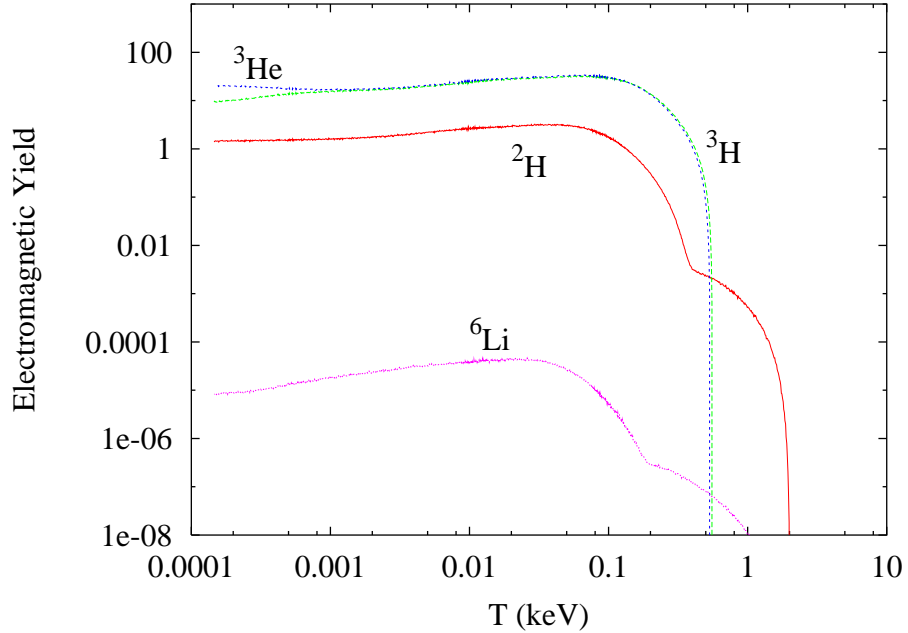


FIG. 4: Yields of (from top to bottom) ^3He (blue), ^3H (green), ^2H (red), and ^6Li (magenta) nuclei per TeV of electromagnetic energy injected (in form of energetic γ -rays and energetic e^\pm) due to photodisintegration reactions (^2H , ^3H , ^3He , and ^6Li) and fusion reactions (^6Li) as a function of cosmic temperature.

Compton scattering (App. E 2b). A substantial though small fraction of ^2H may photodisintegrate either ^4He or ^3H [12]. The reader is referred to Fig. 4 and Fig. 5 for typical light-element production- and destruction- factors during electromagnetic decays. When ^4He photodisintegration becomes important ($> 10^7 \text{ sec}$), photodisintegration of ^2H is a subdominant effect as more ^2H is produced in the relatively larger numbers of ^4He -nuclei which are photodisintegrated. Energetic ^3H and ^3He produced in large numbers during the ^4He photodisintegration may lead via non-thermal fusion reactions to ^6Li [17], similar to the energetic mass three nuclei produced in ^4He spallation during hadronic decays. To a less important degree ^6Li may also be created by direct photodisintegration of ^7Li and ^7Be .

Thus, the effects of injection of electromagnetic interacting particles on BBN yields are due to photodisintegration and are only operative at comparatively late times ($> 10^5 \text{ sec}$). A much simplifying aspect of BBN with electromagnetic interacting particles is the fact that results almost always only depend on the total amount of electromagnetic interacting energy, rather than the energy and nature of the injected primary. This is due to the number of cascade photons and electrons being so large that asymptotically the same state is reached, independent of the initial state. Finally it is noted that hadronic decays (such as $X \rightarrow q\bar{q}$, with q a quark) generically also lead to the injection of electromagnetic interacting primaries, as for example due to 0 's which decay into two photons.

III. OBSERVATIONAL LIMITS ON THE PRIMORDIAL ABUNDANCES

The following provides a compilation of the observational limits on primordial abundances adopted in the present analysis. For more detail on observations and interpretations, the reader is either referred to the original literature or reviews on BBN nucleosynthesis (cf. [25, 26]).

A. ^4He

The primordial ^4He abundance is inferred from observations of hydrogen- and helium-emission lines in extragalactic low-metallicity H II-regions. The two most recent observations yield $Y_p = 0.2421 \pm 0.0021$ [27] and $Y_p = 0.239 \pm 0.002$ [28]. Nevertheless, somewhat smaller $Y_p = 0.2345$ or larger $Y_p = 0.2443$ determinations by the same authors, but determined from (partially) different data sets, have also been cited. The estimates are significantly

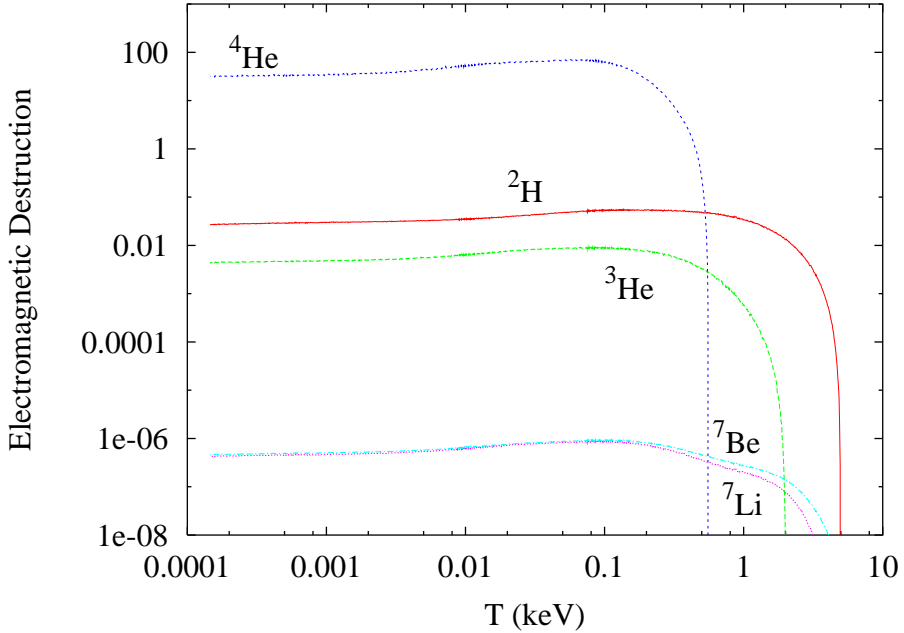


FIG. 5: Number of destroyed (from top to bottom) ^4He (blue), ^2H (red), ^3He (green), and ^7Li (magenta) (^7Be - light blue) nuclei per TeV of electromagnetically interacting energy injected into the primordial plasma at temperature T . For the purpose of illustration we have taken the ^7Li and ^7Be abundances equal at $^7\text{Li}/\text{H} = ^7\text{Be}/\text{H} = 4.34 \cdot 10^{-10}$. In reality it is the sum of both isotopes which is synthesized at $(^7\text{Li} + ^7\text{Be})/\text{H} = 4.34 \cdot 10^{-10}$ in a SBBN scenario at $bh^2 = 0.02233$ with ^7Be being converted to ^7Li by electron capture at cosmic temperatures $T = 0.1 - 1 \text{ keV}$.

below the SBBN Y_p prediction at the WMAP III baryon density. However, the quoted error bars are purely statistical in nature and only some of them may possibly be systematic errors. Systematic errors include underlying stellar absorption, ionization corrections, temperature fluctuations, and collisional excitation. Recent re-analysis of the original data by an independent group [29], has led to a significantly revised $Y_p = 0.249 \pm 0.009$ estimate, including a substantial increase of the error bars. Nevertheless, even this latter study does not include a study of the majority of systematic uncertainties, such that its utility is somewhat questionable. Many of these systematic uncertainties would lead again to a decrease of the inferred Y_p . In a conservative spirit, however, the present analysis utilizes the upper limit as quoted above

$$Y_p < 0.258 : \quad (1)$$

A lower limit on Y_p is not considered as usually of no use for deriving limits on relic decaying particles.

B. ^2H

The most accurate method for an observational determination of the primordial $^2\text{H}/\text{H}$ -ratio is believed to be due to observations of low-metallicity quasar absorption line systems (QALS). Such gaseous systems, on the line of sight between a high redshift quasar and the observer, produce absorption lines in the continuous spectrum of the quasar at the redshifted wavelength of the Lyman- α ^2H and ^1H positions, respectively. If the QALS has a simple velocity structure, the depths of the absorption troughs may be used to infer the $^2\text{H}/\text{H}$ -ratio. As observations focus on systems at very low metallicity, the assumption is typically that only very little stellar ^2H destruction has occurred, and that the determined abundance may be directly compared to the predicted BBN $^2\text{H}/\text{H}$ -ratio. When the currently six best determinations [30] are averaged one obtains a QALS-inferred primordial $^2\text{H}/\text{H}$ abundance of $^2\text{H}/\text{H} = 2.4 \pm 0.4 \cdot 10^{-5}$ [25]. This value compares favorably to that predicted by a SBBN scenario at the WMAP III baryonic density. Nevertheless, caution has to be applied as the intrinsic dispersion between individual central values of $^2\text{H}/\text{H}$ determinations is much larger than most of the quoted error bars for individual QALS. Thus, the highest

individual 2- upper limit and the lowest individual 2- lower limit of all six systems span a range

$$1.2 \times 10^{-5} < {}^2\text{H}/\text{H} < 5.3 \times 10^{-5}; \quad (2)$$

much larger than the above quoted error bar. Furthermore, a systematic trend of decreasing ${}^2\text{H}/\text{H}$ with increasing column density N_{H} of the QALS may be found indicating the existence of possible systematic errors. Assuming to remain on the conservative side the above range is adopted in the analysis for an acceptable ${}^2\text{H}/\text{H}$ abundance. Conservatism may be in order not only because a recent proposal of a very active stellar Pop III population, which could potentially reduce the primordial ${}^2\text{H}/\text{H}$ -ratio in certain (high N_{H}) systems without much trace of associated iron or silicon production [7].

C. ${}^3\text{He}/{}^2\text{H}$

Precise observational determinations of ${}^3\text{He}/\text{H}$ -ratios are only possible within our galaxy. Since our galaxy is chemically evolved, it is difficult to make a straightforward connection to the primordial ${}^3\text{He}/\text{H}$ abundance. Since ${}^3\text{He}$, in fact, is known to be destroyed in some stars, but produced in others, observed ${}^3\text{He}/\text{H}$ -ratios may also only with difficulty be utilized to obtain an upper or lower limit on the primordial ${}^3\text{He}/\text{H}$. This is in contrast to the ${}^3\text{He}/{}^2\text{H}$ -ratio. ${}^2\text{H}$ is known to be always destroyed in stars (in fact is burned into ${}^3\text{He}$), whereas ${}^3\text{He}$ is either destroyed or produced. The cosmic ${}^3\text{He}/{}^2\text{H}$ -ratio may therefore only increase with time. Thus a determination of this ratio in any environment, even chemically evolved, may be taken as an upper limit on the primordial ${}^3\text{He}/{}^2\text{H}$ -ratio [31]. From a combination of solar wind observations and the planetary gas component of meteorites and Jupiter, it is possible to infer the ${}^3\text{He}/\text{H} = 1.66 \pm 0.05 \times 10^5$ and ${}^2\text{H}/\text{H} = 1.94 \pm 0.39 \times 10^5$ -ratios at the time of solar system formation independently [32]. Employing the 2- upper end of the ${}^3\text{He}$ abundance and the 2- lower end of the ${}^2\text{H}$ abundance, when may derive a conservative constraint of

$${}^3\text{He}/{}^2\text{H} < 1.52; \quad (3)$$

for the primordial ${}^3\text{He}/{}^2\text{H}$ ratio.

D. ${}^7\text{Li}$

For a long time it has been known that the ${}^7\text{Li}/\text{H}$ -ratio in the atmospheres of low metallicity Pop II stars is essentially constant with metallicity (the Spite plateau) with deduced central values on the plateau falling in the range $1.23 \times 10^{-10} < {}^7\text{Li}/\text{H} < 1.73 \times 10^{-10}$ [33]. As this value is traditionally interpreted to be close to the primordial ${}^7\text{Li}/\text{H}$ -ratio, a factor 2-3 discrepancy between the SBBN predicted primordial ${}^7\text{Li}/\text{H}$ at the WMAP III baryon density (usually in excess of 4×10^{-10}) and that inferred from the stars on the Spite plateau is apparent. This situation has neither been changed by a large number of re-evaluations of the ${}^7\text{Li}/\text{H}$ -abundance of the Spite plateau, nor convincingly shown to be solved by stellar depletion of ${}^7\text{Li}$. As the ${}^7\text{Li}$ isotope is not very important in constraining relic decaying particles (rather, it may resolve the problem), the reader is referred elsewhere for discussion of this problem (e.g. [7, 9, 25]). The present analysis adopts only a lower limit on the primordial ${}^7\text{Li}/\text{H}$

$${}^7\text{Li}/\text{H} > 0.85 \times 10^{-10}; \quad (4)$$

chosen by the 95% confidence level lower limit as derived by Ref. [34].

E. ${}^6\text{Li}$

The isotope of ${}^6\text{Li}$ can be particularly useful in deriving constraints on relic decaying particles [17]. Recently, the number of claimed preliminary detections of ${}^6\text{Li}/{}^7\text{Li}$ -ratios in low metallicity Pop II stars has multiplied by a large factor [24] (cf. to Ref. [35] for the few former detections) falling in the range $0.03 < {}^6\text{Li}/{}^7\text{Li} < 0.07$ with average ${}^6\text{Li}/{}^7\text{Li} = 0.042$ and with no star having ${}^6\text{Li}/{}^7\text{Li}$ in excess of 0.1. The origin of this ${}^6\text{Li}$ is unknown. Concerning a limit on the primordial ${}^6\text{Li}$ -abundance the situation is somewhat problematic. This is particularly so, since the predicted SBBN ${}^7\text{Li}$ is in excess of that observed. If this latter fact is after all explained by stellar ${}^7\text{Li}$ destruction, ${}^6\text{Li}$ would

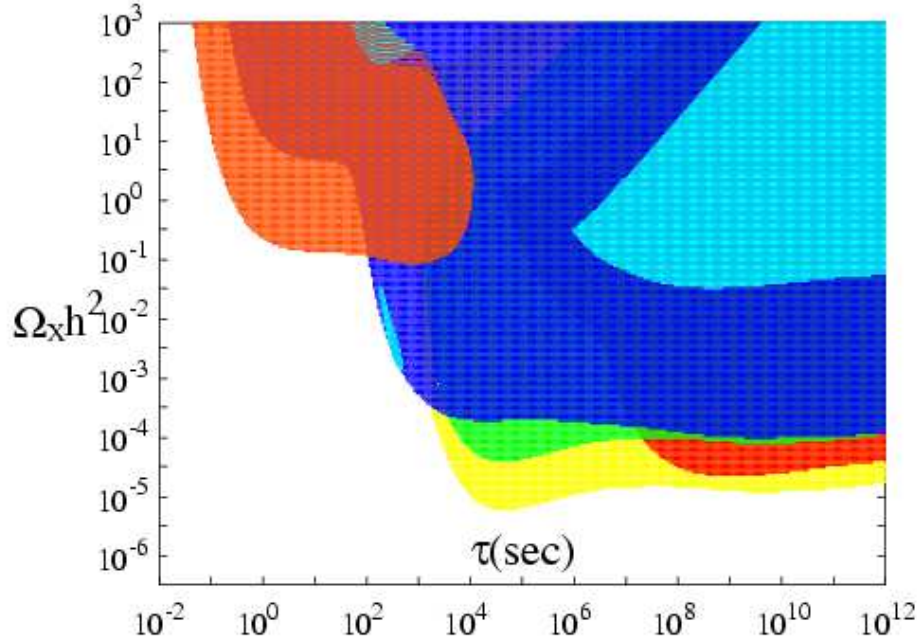


FIG . 6: Conservative BBN constraints on the abundance of relic decaying particles as a function of their life time for a $M_x = 1 \text{ TeV}$ particle with hadronic branching ratio $B_h = 1$. Lim its are given on the contribution the decaying particles would have made to the present critical density, $\Omega_X h^2$ (with h the Hubble parameter), if they would have not decayed. For a conversion to constraints on, for example $M_x n_x = n$ the reader is referred to App. A. The colored regions are excluded and correspond to the constraints imposed by the observationally inferred upper limit on ^4He - orange - (Eq. 1), upper limit on ^2H - blue - (Eq. 2), upper limit on $^3\text{He}/^2\text{H}$ - red - (Eq. 3), and lower limit on ^7Li - light blue - (Eq. 4). Conservative constraints derived from $^6\text{Li}/^7\text{Li}$ (Eq. 6) are shown by the green region. The region indicated by yellow violates the less conservative $^6\text{Li}/^7\text{Li}$ (Eq. 5) constraint but should not be considered ruled out. Rather, this region may be cosmologically interesting as a putative source of ^6Li in low-metallicity stars by relic decaying particles.

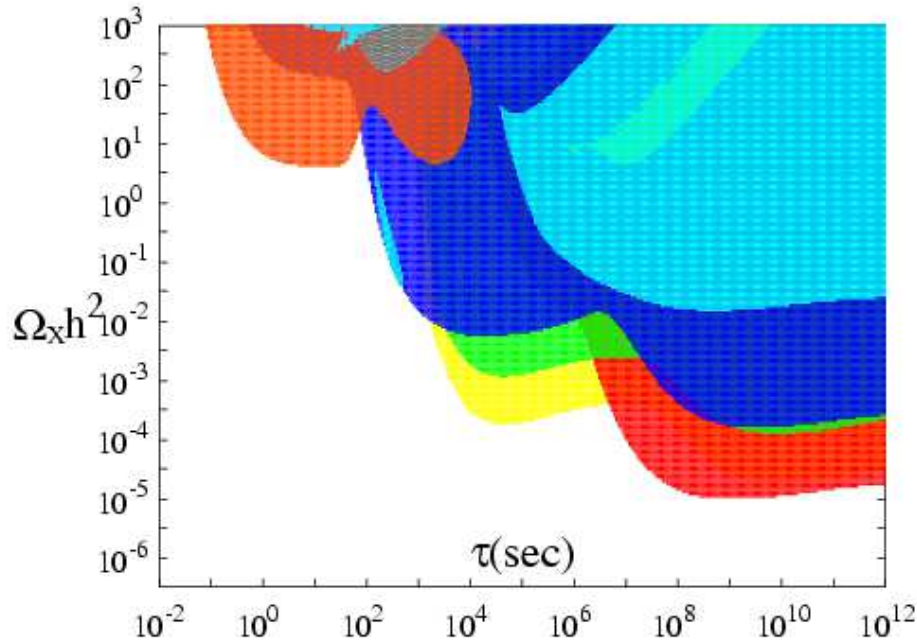


FIG . 7: As Fig. 6 but for hadronic branching ratio $B_h = 3.33 \times 10^{-2}$.

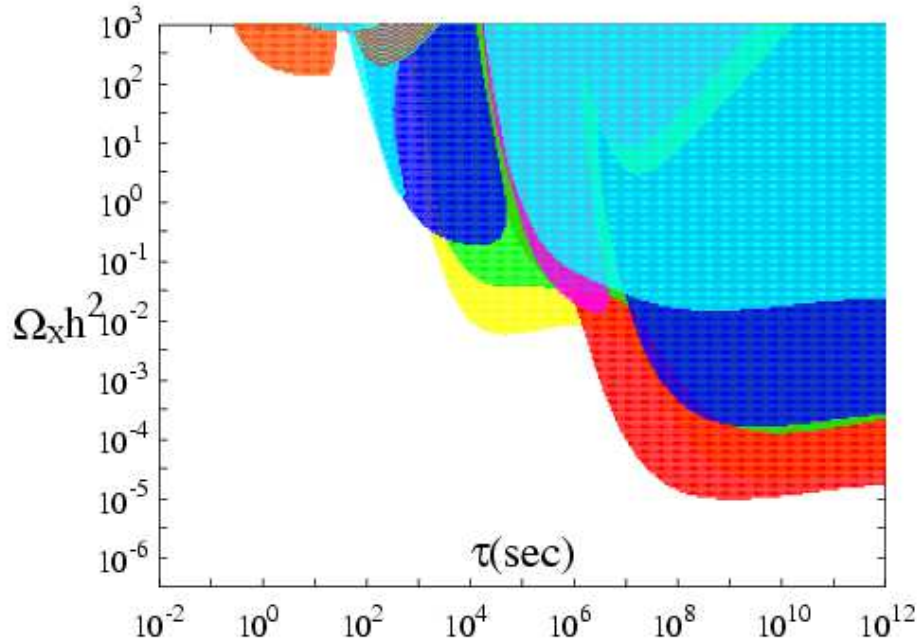


FIG. 8: As Fig. 6 but for hadronic branching ratio $B_h = 10^{-3}$. The region excluded by the lower limit on $^2\text{H}/\text{H}$ (Eq. 2) is indicated by the color magenta.

also be destroyed. In the best case (destroying as little as possible ^6Li), both the ^6Li and ^7Li abundances would be destroyed by the same factor, with their ratio, nevertheless, staying constant. In this case one may adopt

$$^6\text{Li}/^7\text{Li} < 0.1 \quad (5)$$

as upper limit. This would correspond to a primordial $^6\text{Li}/\text{H} < 4.34 \cdot 10^{-11}$ (given that the SBBN prediction is $4.34 \cdot 10^{-10}$ in the present analysis, cf. App F) already much in excess of the 2- upper limit of $^6\text{Li}/\text{H} < 1.47 \cdot 10^{-11}$ in the well studied star HD 84937. However, calculations of ^6Li and ^7Li destruction in stars generally predict more ^6Li destruction than ^7Li destruction, since ^6Li is more fragile than ^7Li . In Ref. [3] which studied ^7Li depletion in rotating stars a correlation between the amount of ^7Li and ^6Li destruction was obtained, with, for example, factor 2 (4) reduction of the $^6\text{Li}/^7\text{Li}$ ratio occurred for factor 1.6 (2.5) reduction of the ^7Li abundance. When the (ne tuned) models by Ref. [4] are taken, designed to explain a larger amount of ^7Li destruction without spoiling the atness of the Spite plateau (when plotted against stellar temperature), a factor 1.6 (2.5) of ^7Li destruction implies a factor 1.25 (1.58) reduction in the $^6\text{Li}/^7\text{Li}$ ratio. Particularly the last destruction factor would render the ^6Li isotope not anymore as useful in deriving limits on decaying particles. Nevertheless, in the spirit of a conservative study we will also adopt

$$^6\text{Li}/^7\text{Li} < 0.66 \quad \text{conservative}; \quad (6)$$

as a second more conservative limit. Here this value derives by taking the average observed $^6\text{Li}/^7\text{Li}$ ratio of 0.042 and multiplying it by the $^6\text{Li}/^7\text{Li}$ destruction factor of 15.8. This is done with the understanding that any models which violate Eq. (5) but not Eq. (6) should be flagged as potentially being ruled out. On the other hand, such models, if not violating other observational constraints, could also explain the origin of the observed ^6Li (cf. Ref. [8, 9]).

IV. CONSTRAINTS ON RELIC DECAYING PARTICLES

In this section conservative constraints on the abundance of putative relic decaying particles in the early Universe are presented. The number density n_X of an early produced semi-stable particle species X with decay width $\Gamma_X = 1 = \Gamma_X$ follows the equation

$$\frac{dn_X}{dt} = -3H n_X - \frac{n_X}{\Gamma_X}; \quad (7)$$

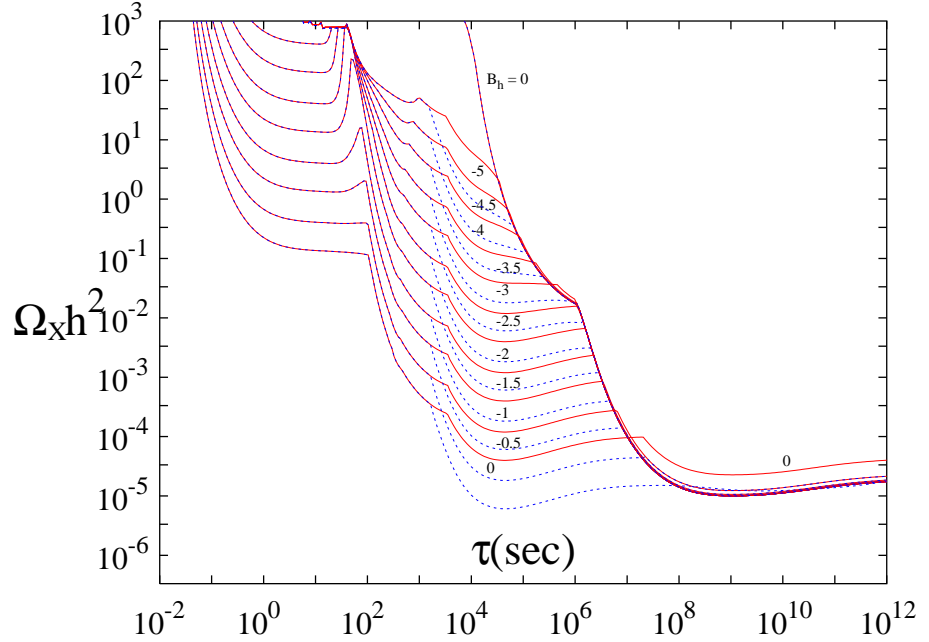


FIG. 9: Constraints on the abundance of decaying particles as a function of life time for an $M_x = 1$ TeV particle with varying hadronic branching ratios. Constraints are shown for hadronic branching ratios (from bottom to top) $\log_{10} B_h = 0, 0.5, 1, -1.5, -2, -2.5, -3, -3.5, -4, -4.5$, and -5 , respectively, as labeled. The case $B_h = 0$ is also shown. The labels always correspond to the solid (red) line above it. For each B_h , the region above this solid (red) line is ruled out when conservative constraints are applied (i.e. Eqs 1-4 and 6). When the ${}^6\text{Li}/{}^7\text{Li}$ constraint Eq. 6 is replaced by the less conservative Eq. 5 the dotted (blue) constraint lines result. These dotted lines coincide for small and large x with the solid (red) lines.

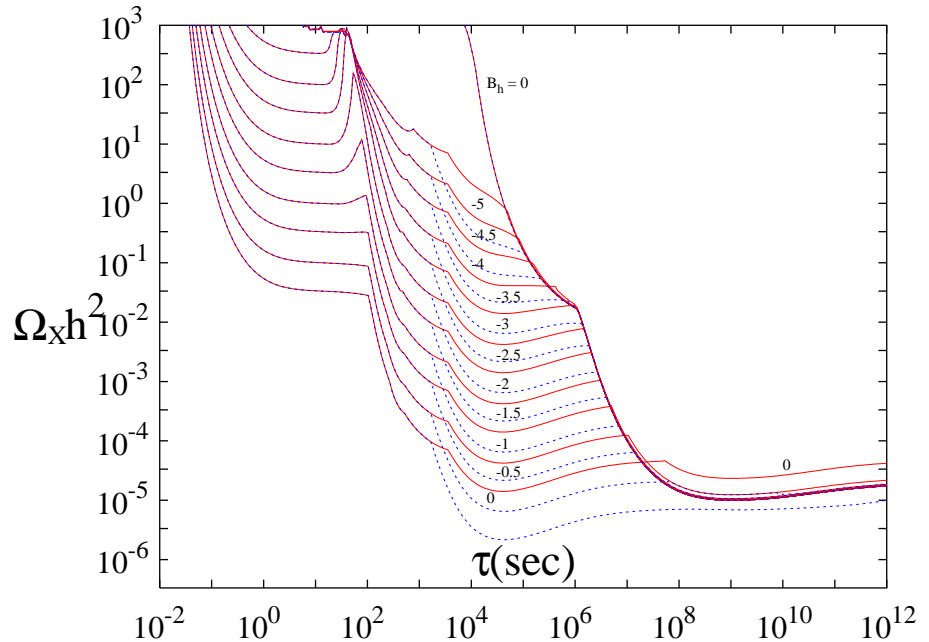


FIG. 10: As Fig. 9 but for $M_x = 100$ GeV.

where t is cosm ic time and H is the Hubble constant. Here the first term on the right-hand-side describes dilution due to cosm ic expansion, whereas the second term represents the particle decay. Results are presented for a large number of di erent hadronic branching ratios B_h of the particle X . In particular, it is assumed that a fraction B_h of all decays are hadronic and a fraction $1 - B_h$ are electrom agnetic. During hadronic decays the prim aries injected into the plasma are assumed to be a quark-antiquark pair of total energy M_x and total momentum zero in the cosm ic rest fram e. The hadronization of the q-q ux tube is followed with aid of the code PYTHIA, resulting in numerous nucleons, mesons, e and -rays injected into the plasma. Note that for large M_x , as considered here, the spectrum of the resulting post-hadronization particles is virtually independent of the type of initial quark injected. As already stated in Sec. II, for su ciently massive particles X the e ects of electrom agnetic decays on BBN yields depends only on the total energy E_e , in e and -rays injected into the plasma. For electrom agnetic decays $E_e^{\text{EM}} = M_x$ is thus assumed with no injection of nucleons or mesons. Hadronic decays are also associated with the release of energetic electrom agnetically interacting particles. Following results from PYTHIA $E_e^H = 0.45M_x$ is taken. Finally, it is noted that only baryon number conserving decays are considered.

In Figs 6-8 constraints on the abundance of $M_x = 1 \text{ TeV}$ relic decaying particles for hadronic branching ratios $B_h = 1$, $B_h = 3.33 \cdot 10^{-2}$, and $B_h = 10^{-3}$, respectively, are shown. The colored (shaded) regions are excluded, with di erent colors (shades) corresponding to constraints derived from di erent light elements, as indicated in the figure captions. It is evident that the most stringent constraints derive from an overproduction of ^4He at early times $x < 10^2 \text{ sec}$, an overproduction of ^2H in the decay time interval $10^2 \text{ sec} < x < 10^3 \text{ sec}$, an overproduction of ^6Li in the decay time interval $10^3 \text{ sec} < x < 10^7 \text{ sec}$, and an overproduction of the $^3\text{He}/^2\text{H}$ -ratio for large decay times $x > 10^7 \text{ sec}$. The yellow area in the gures corresponds to elevated ^6Li production in the range $0.1 < ^6\text{Li}/^7\text{Li} < 0.66$ and should currently not be considered ruled out. Though in excess of the observationally inferred $^6\text{Li}/^7\text{Li}$ abundance ratio in low-m etallicity stars it is conceivable that some of the produced ^6Li has been destroyed in low-m etallicity stars. The reader is referred to Sec. III E for details. In contrast, as the source of the unexpected large abundance of ^6Li in low-m etallicity stars is unknown, the yellow region may be considered as cosm ologically interesting [8, 9].

In Figs 9-10 constraints on the abundance of relic decaying particles for a large number of hadronic branching ratios and two di erent particle masses, $M_x = 100 \text{ GeV}$ and $M_x = 1 \text{ TeV}$ are shown. The region above the solid (red) lines for each particular B_h are excluded. The gure also shows by the dotted (blue) lines how the constraints would change if one were to replace the observationally inferred limit on $^6\text{Li}/^7\text{Li}$ in Eq. 6 by the less conservative constraint Eq. 5. However, as argued above, the latter constraint should currently not be applied.

V . CONCLUSIONS

BBN is a powerful probe of the conditions in the early Universe and may severely limit the putative existence of relic decaying particles. In this paper, the e ects of electrom agnetically and hadronically decaying particles on the BBN light-element synthesis of ^2H , ^3He , ^4He , ^6Li , and ^7Li have been considered in detail. All processes which the author believes to play a role at the 10% level have been included. These include nucleon-nucleon elastic and inelastic scatterings, nucleon-antinucleon annihilation, spallation of ^4He by energetic nucleons, fusion reactions of ^3H and ^3He on ^4He nuclei, mesonic charge exchange, Coulomb- and magnetoolement scattering, Thomson scattering, Bethe-Heitler pair production, photon-photon scattering, (inverse) Compton scattering, and photodisintegration of light nuclei, among others. The analysis attempts to stay as close as possible to existing experimental data. A number of expressions, as for example the Coulomb stopping power of comparatively slow nuclei have been newly evaluated. All these non-therm al reactions are coupled to the thermonuclear fusion reactions known to be of importance during BBN. Results of such complete calculations have been first presented in Ref. [8, 20] and particularly, Ref. [21], nevertheless, only for a limited number of decaying particle properties.

Predicted light-element yields are compared to observationally inferred limits on primordial light-element abundances to infer accurate and conservative limits on electrom agnetically and hadronically decaying particles in the early Universe. Constraints on the abundance of such decaying particles are shown for a large number of hadronic branching ratios and particles masses. This was necessary to obtain comparatively accurate limits as a simple extrapolation between the results of only two hadronic branching ratios may yield to erroneous or inaccurate results. The results in this paper may be used to further constrain the evolution of the very early Universe.

TABLE I:

No.	Reaction	Channel	Ref.	No.	Reaction	Channel	Ref.
1	$p + e^- !$ elastic	Coulomb	App. D 1a	48	$p + p !$	elastic	[44, 45], App. E 3
2	$p(N) + \text{CMBR} !$	Thomson	App. D 1b	49	$p + {}^4\text{He} !$	elastic	[44], App. E 3
3	$n + e^- !$	magnetic moment	App. D 1c	50	$n + p !$	elastic	[44, 45], App. E 3
4	$+ \text{CMBR} !$	$e^- + e^+$	App. D 2	51	$n + {}^4\text{He} !$	elastic	[44], App. E 3
5	$e^- + \text{CMBR} !$	inverse Compton	App. D 2, D 2b	52	$p + p !$	$p + p + {}^0$	[46], App. E 4
6	$+ p({}^4\text{He}) !$	$p({}^4\text{He}) + e^- + e^+$	App. D 2a	53		$n + p + {}^+$	[46, 47], App. E 4
7	$+ e^- !$	Compton	App. D 2c	54		${}^2\text{H} + {}^+$	[46, 47], App. E 4
8	$+ \text{CMBR} !$	+	App. D 2d	55		$p + p + {}^+$	[46], App. E 4
				56		${}^2\text{H} + {}^+ {}^0$	[46], App. E 4
9	$+ {}^2\text{H} !$	$p + n$	[36]	57		${}^2\text{H} + {}^2 {}^+$	[46], App. E 4
10	$+ {}^3\text{H} !$	${}^2\text{H} + n$	[36]	58		$p + p + {}^+ {}^0$	[46], App. E 4
11		$2n + p$	[36]	59		$n + p + {}^2 {}^+$	[46], App. E 4
12	$+ {}^3\text{He} !$	${}^2\text{H} + p$	[36]	60		$p + p + {}^2 {}^0 + ({}^0\text{s})$	[46, 47], App. E 4
13		$2p + n$	[36]	61		$n + n + {}^2 {}^+ + ({}^0\text{s})$	[46], App. E 4
14	$+ {}^4\text{He} !$	${}^3\text{H} + p$	[36]	62		$n + p + {}^+ + ({}^0\text{s})$	[46, 47], App. E 4
15		${}^3\text{He} + n$	[36, 37]	63	$n + p !$	$p + n + {}^0 + ({}^0\text{s})$	[46], App. E 4
16		${}^2\text{H} + {}^2\text{H}$	[36]	64		${}^2\text{H} + {}^0 + ({}^0\text{s})$	[46], App. E 4
17		${}^2\text{H} + n + p$	[36]	65		$p + p +$	[46], App. E 4
18	$+ {}^6\text{Li} !$	${}^4\text{He} + n + p$	[36, 38]	66		$n + n + {}^+$	[46], App. E 4
19		${}^3\text{A} + X$	[36]	67		$n + p + {}^+$	[46, 47], App. E 4
20	$+ {}^7\text{Li} !$	${}^4\text{He} + {}^3\text{H}$	[36, 39]	68		$p + p + {}^0 + ({}^0\text{s})$	[46], App. E 4
21		${}^6\text{Li} + n$	[36]	69		${}^2\text{H} + {}^+$	[46], App. E 4
22		${}^4\text{He} + 2n + p$	[36]	70		$n + n + {}^+ + ({}^0\text{s})$	[46, 47], App. E 4
23		${}^4\text{He} + {}^2\text{H} + n$	App. D 3	71		$n + p + {}^2 {}^+ + ({}^0\text{s})$	[46], App. E 4
24		${}^6\text{He} + p !$ ${}^6\text{Li} + p$	App. D 3	72		$n + p + {}^+ {}^0$	[46], App. E 4
25		${}^2\text{H} + p$	App. D 3	73		$p + p + {}^2 {}^+$	[46], App. E 4
26		${}^3\text{H} + {}^3\text{He} + n$	App. D 3				
27	$+ {}^7\text{Be} !$	${}^4\text{He} + {}^3\text{He}$	[36, 43]	74	$p + {}^4\text{He} !$	${}^3\text{H} + {}^2\text{p} + ({}^s)$	App. E 5, E 6
28		${}^6\text{Li} + p$	[36]	75		${}^3\text{He} + n + p + ({}^s)$	App. E 5, E 6
29		${}^4\text{He} + 2p + n$	[36]	76		${}^2\text{H} + {}^2\text{p} + n + ({}^s)$	App. E 5
30		${}^4\text{He} + {}^2\text{H} + p$	App. D 3	77		${}^3\text{He} + {}^2\text{H}$	App. E 5, E 6
31		${}^6\text{Be} + n !$ ${}^4\text{He} + 2p + n$	App. D 3	78		${}^2\text{H} + {}^2\text{H} + p + ({}^s)$	App. E 5
32		${}^2\text{H} + n$	App. D 3	79	$n + {}^4\text{He} !$	${}^3\text{He} + 2n + ({}^s)$	App. E 5, E 6
33		${}^3\text{H} + {}^3\text{He} + p$	App. D 3	80		${}^3\text{H} + n + p + ({}^s)$	App. E 5, E 6
				81		${}^2\text{H} + {}^2\text{n} + p + ({}^s)$	App. E 5
34	$+ n !$	${}^0 ({}^0) + p$	[15], App. E 1	82		${}^3\text{H} + {}^2\text{H}$	App. E 5, E 6
35	$+ p !$	${}^0 ({}^0) + n$	[15], App. E 1	83		${}^2\text{H} + {}^2\text{H} + n + ({}^s)$	App. E 5
36	$K + n !$	$p + X$	[15], App. E 1	84	$p + {}^6\text{Li} !$	${}^3\text{He} + {}^4\text{He}$	App. E 5
37		$n + X$	[15], App. E 1				
38	$K + p !$	$n + X$	[15], App. E 1	85	${}^3\text{H} + {}^4\text{He} !$	${}^6\text{Li} + n$	App. E 6
39		$p + X$	[15], App. E 1	86	${}^3\text{He} + {}^4\text{He} !$	${}^6\text{Li} + p$	App. E 6
40	$K_L + n !$	$p + X$	[15], App. E 1	87	${}^4\text{He} + {}^4\text{He} !$	${}^6\text{Li} + {}^2\text{H}$ (${}^6\text{Li} + p + n$)	App. E 6
41		$n + X$	[15], App. E 1	88		${}^7\text{Li} + p$ (${}^7\text{Be} + n$)	App. E 6
42	$K_L + p !$	$n + X$	[15], App. E 1				
43		$p + X$	[15], App. E 1	89	${}^3\text{He} + p !$	elastic	App. E 6
				90	${}^3\text{H} + p !$	${}^3\text{He} + n$	App. E 6
44	$p + p !$'s	[15], App. E 2	91	${}^3\text{H} + p !$	elastic	App. E 6
45	$n + p !$'s	[15], App. E 2	92	${}^3\text{H} !$	${}^3\text{He} + e^- + e^-$	[58], App. E 6
46	$p + n !$'s	[15], App. E 2	93	${}^7\text{Be} + e^- !$	${}^7\text{Li} + e^-$	[58]
47	$n + n !$'s	[15], App. E 2				

A cknow ledgm ents

I acknowledge useful exchanges with D . A mdt, M . A splund, A . Blinov, J. Bystricky, R . Cyburt, M . Chadeyeva P . D escouvement, E . Keihanen, H .P . M orsch, K . O live, N . P rantzos, O . R ichard, E . VangioniF lam .

A P P E N D I X A : G E N E R A L C O N S I D E R A T I O N S

For the computation of light-element abundance yields in the presence of decaying or annihilating relic particles during or after BBN one has to essentially treat the thermalization process of energetic nucleons, antinucleons, and γ -rays. These latter particles result as primaries from the decay/annihilation process. Their thermalization occurs due to a host of processes discussed in detail in App. D and E. At the same time, thermal nuclear reactions of the thermal baryonic component may play a role at high temperatures $T > 10$ keV. In general, the problem simplifies considerably due to two facts: (a) thermalization may be treated as an instantaneous process on the Hubble time scale and (b) interactions between two non-thermal nucleons/nuclei are improbable. Given a typical proton density $n_p = 1.6 \cdot 10^6 \text{ cm}^{-3}$ ($T = 10$ keV)³ and a typical nucleon (nuclei)-nucleon interaction cross section of 30 mb and 300 mb at nucleon (nuclei) kinetic energy $E_k = 1$ GeV and 10 MeV, respectively, one finds a typical scattering time $\tau_N = 0.07 \text{ sec}$ ($T = 10$ keV)³ which is approximately constant with kinetic energy. This may be compared to the Hubble time $\tau_H = 1.4 \cdot 10^6 \text{ sec}$ ($T = 10$ keV)² to yield a ratio $\tau_N = \tau_H = 5 \cdot 10^5$ ($T = 10$ keV)¹ where it is approximated that it takes around ten scatterings for the complete thermalization of a nucleon. It is seen that only at very low temperatures $T < 0.1$ eV thermalization may not be regarded instantaneous on the Hubble scale. Due to the short survival times of energetic nucleons (nuclei) only for excessively large ratios of non-thermalized-to-thermalized nucleons $\text{non-thermal} = b = 10^6$ ($T = 10$ keV) interactions between two non-thermalized nucleons become important. For such large non-thermal, however, BBN (almost) always fails badly in predicting the observationally inferred primordial abundances, such that such interactions may be neglected.

Abundance yields due to decaying particles may be often understood as the product of individual factors. For example, for the production of ^6Li nuclei by the fusion reactions 85 and 86, induced by non-thermalismass-3 nuclei, one may schematically write the final number of produced ^6Li nuclei $N^{^6\text{Li}}$, produced during a certain cosmic expansion interval $\ln a$

$$N^{^6\text{Li}} = \frac{Z}{dN^{^6\text{Li}}} = \frac{Z}{d\ln a} \frac{dD \text{ decays}}{d\ln R} \frac{n_{p,n}}{D \text{ decay}} \frac{n_3}{n_{p,n}} \frac{n_6}{n_3} ; \quad (\text{A 1})$$

where a denotes the cosmic scale factor. Here the integrand is composed of the number of relic particle decays per logarithmic scale factor interval, times the number of energetic nucleons produced per decay, times the number of energetic ^3H and ^3He produced during the thermalization of a nucleon, times the fraction of ^3H and ^3He nuclei which fuse to form ^6Li . Similarly there are contributions from photodisintegration not shown in Eq. A 1. The present analysis treats in detail the third and fourth factors, pertaining to thermalization. For example, the last factor in the integrand ($n_6 = n_3$) may be seen in Fig. 2 for various cosmic temperatures. The second factor is given by an assumed initial post decay state (e.g. qq an energetic quark-antiquark-uxtube at an assumed energy) in combination with the results of an hadronization code, such as PYTHIA, which computes the number and energy of produced (anti)nucleons, mesons, and γ -rays after hadronization of the initial qq-uxtube. This factor ($n_{p,n} = D \text{ decay}$) convolved with ($n_3 = n_{p,n}$) may be seen in Fig. 3 (cf. also to Fig. 4 for a similar convolution due to photodisintegration). Finally, the first factor is given by the assumed abundance and life time of the putative relic.

All figures in the main text limit $x h^2$, the contribution of the decaying particle density to the present critical density x if the particle were not decaying. Here h is the present Hubble constant in units of $100 \text{ km s}^{-1} \text{Mpc}^{-1}$. Other studies often present limits on the number of X -particles per photon times M_x , the mass of the X -particle, or the number of X -particles per radiation entropy times M_x . The conversion factors between these quantities are given by ${}_1 = n_X M_x = n = 2.5784 \cdot 10^{-8} \text{ GeV}^{-1} h^2$ and ${}_2 = n_X M_x = s = 3.6639 \cdot 10^{-9} \text{ GeV}^{-1} h^2$.

A P P E N D I X B : N U M E R I C A L M O N T E - C A R L O P R O C E D U R E

The present analysis utilizes a Monte-Carlo approach to the problem. At each time step of the order of 10^4 non-thermal nucleons and $6 \cdot 10^3$ γ -rays are injected into the thermal plasma. Here the initial energies are randomly drawn, in the case of nucleons, from a kinetic energy distribution function generated by PYTHIA, and in the case of

photons, from the distribution function given in Eq. D.8. Mesons, which to a large part thermalize before interacting are injected in their number ratios predicted by PYTHIA. The subsequent evolution of each nucleon is followed by a Monte-Carlo (random probabilistic) sequence of events. Energy losses of nucleons are determined by a competition between nuclear scattering (spallation) processes (App. E.3 – E.5), in which a nucleon may lose a good part of its energy, and continuous energy losses, such as Coulomb stopping, Thomson scattering, and magnetic moment scattering (App. D.1). The probability of survival of a nucleon (nuclei) k against nuclear scattering while it loses continuously energy between energy E_i and E_f is given by

$$P_k(E_i \text{ to } E_f) = \exp \left(-\frac{\int_{E_i}^{E_f} \frac{dE}{\lambda_N(E)} dx_j}{\lambda_N(E_f) dx_j} \right) \quad (B1)$$

where dx_j is the energy-dependent continuous energy loss per unit path length and $\lambda_N^{-1} = \frac{1}{\lambda_N(E_f) dx_j} = \frac{1}{\lambda_N(E_f) dx_j}$ is the inverse of the nucleon (nuclei) mean free path against nuclear scattering. This probability distribution is mapped in the analysis by utilizing random numbers. Further, the evolution of any secondary energetic nucleons due to nuclear scattering is followed as well. The thermalization of nucleons is followed down to energies below which inelastic processes are not anymore possible. The remainder of the thermalization occurs quickly through elastic processes and does not further influence the BBN yields. In Fig. 1 an approximation to the integrand in Eq. B1 may be seen for protons and neutrons at various temperatures.

Photons are treated in a similar way. Each injected photon and the thereby produced secondaries are followed in a Monte-Carlo way until all photons have dropped below the lowest photodisintegration threshold. The number of nuclei (nucleons) A per decaying particle X produced due to all γ -rays created as a consequence of the decay of X are computed via

$$\frac{N_A}{\text{Decay}} = \sum_i \frac{dN(E_i)}{dE_i} E_i \sum_B \sum_j n_B \lambda_B(E_i) \lambda_{A \rightarrow C_j}(E_j) n_A \lambda_A(E_j) \quad (B2)$$

Here the sum over index i runs over the energy spectrum of the initial (after CMBR cascade) γ -ray spectrum, λ are photodisintegration cross sections, c is the speed of light, and $\lambda_j(E_j)$ are γ -ray survival times against the processes discussed in App. D.2.a, D.2.c, D.2.d, and D.3. The sums over i and j are different due to the inclusion of secondary photons. In particular, a photon with initial energy E_i may produce secondary photons j due to the processes described in App. D.2. The sum over j thus includes all γ 's, primary and secondary, tertiary, ... as long as they are above the photodisintegration threshold. Individual survival times are generated by a Monte Carlo and the γ -ray survival probability $P(E) = \exp(-c \lambda(E))$, with $\lambda(E)$ the mean free path. Finally, it is noted that for accuracy reasons the initial first-generation photon spectrum Eq. D.8 is sampled by an equal amount of photons above and below the photodisintegration threshold for ^4He . This was necessary as otherwise much larger ($\sim 10^3$) numbers of photons would have to be followed in order to obtain accurate result.

APPENDIX C: KINETIC RELATIONS

For the convenience of the author this appendix presents some kinematic relations required to convert cross section data presented in terms of center-of-mass (CM) quantities to cross section data in the laboratory (L) frame of reference. For the energy gain of particle 2 (initially at rest) in elastic $2 \rightarrow 2$ scattering, and given the scattering angle in the CM frame, one finds

$$E_{L,2} = \frac{2}{v_{CM}} v_{CM}^2 M_2 (1 - \cos \theta_{CM}) \quad (C1)$$

where $v_{CM} = p_L^1 = (M_2 + M_1 + E_{L,kin}^1)^{1/2}$, $E_{CM,2} = v_{CM} M_2$, and $p_{CM,j} = v_{CM} v_{CM} M_2$. (Note that $p_{CM,j}$ is invariant during elastic scattering.) Concerning inelastic endothermic $2 \rightarrow 2$ scattering reactions $1 + 2 \rightarrow 3 + 4$ with 2 initially at rest (e.g. reactions 77, 82, 85–88) the threshold in the laboratory system is given by $E_L^1 = m(1 + m_1 + m_2)$ with $m = (m_3 + m_4 - m_1 - m_2)$, the mass differences. During inelastic $2 \rightarrow 2$ scattering with particle 2 initially at rest, $p_{CM,j}$ is not anymore invariant due to conversion of kinetic energy to rest energy. Utilizing the above given (before scattering) $v_{CM}, p_{CM,j}$ relations one may solve the implicit equation $E_{CM}^1 + E_{CM}^2 = E_{CM}^3 + E_{CM}^4$ for p_{CM}^0 , with E_{CM}^3 and E_{CM}^4 containing the after scattering modified p_{CM}^0 . Provided one has θ_{CM} the CM scattering angle, the laboratory energy of particles 3 and 4 are determined by $E_L^3 = v_{CM} (E_{CM}^3 + v_{CM} p_{CM}^0 \cos \theta_{CM})$ and similarly for particle 4 with $v_{CM} \neq v_{CM}$.

APPENDIX D : NON-THERMAL ELECTROMAGNETIC INTERACTIONS

1. Electromagnetic Stopping of N on thermal Nucleons

a. Coulomb interactions

Stopping of charged protons and nuclei by Coulomb scatterings of ambient electrons (and positrons) as well as excitation of collective plasma modes (involving a larger number of electrons) is particularly important. In the early Universe single particle scatterings of electrons and positrons dominate. Since many of these occur with only small momentum transfer (i.e. small-angle scatterings) the process may be regarded as a continuous energy loss for protons and nuclei. Following Jackson [48], Gould [49], and own calculations the energy loss per unit path length traveled may be found

$$\frac{dE_C}{dx} = \frac{Z^2}{v^2} \gamma_p^2 \ln \frac{0.76v}{\gamma_p b} + \frac{1}{2} v^2 ; \quad (D1)$$

where

$$\gamma_p^2 = \frac{4 n_e}{m_e} ; \quad (D2)$$

is the square of the plasma frequency, and

$$b = \max \frac{Z}{m_e v^2} ; \frac{1}{m_e v} ; \quad (D3)$$

In these expressions Z , v , and G refer to electric charge number, velocity, and gamma-factor of the nuclei, respectively, m_e is the electron mass, the ne structure constant, and n_e the total number density of electrons and positrons. This latter is given by

$$n_e = n_{e,net}^2 + n_{e,pair}^2 \stackrel{1=2}{=} \text{with } n_{e,pair} = \frac{1}{2} \frac{2}{m_e T} \stackrel{3=2}{=} e^{m_e T} \frac{1}{1 + \frac{15T}{8m_e}} ; \quad (D4)$$

where T is cosmic temperature. Here $n_{e,net}$ refers to the electrons needed for charge neutrality of the Universe. Eq. (D4) is only accurate in the $T=m_e$ limit. Note that the second term in Eq. (D1) derives from the magnetic momentum scattering contribution of the electron absent in the Rutherford scattering cross section but present in the correct Mott scattering cross section. Note also that, in contrast to the findings of Ref. [15] it is found that Eq. (D1) is also valid in the extremely relativistic limit up to $M_p=m_e$, where M_p is the proton mass. Nevertheless, an important modification to Eq. (D1) occurs for small nuclear velocities and large temperatures when the nuclear velocity v falls below the typical electron velocity v_e . In this case the Coulomb stopping power decreases by a factor $v_e=v^3$ [15], a very large factor 500 for, example, for tritium nuclei of 10 MeV kinetic energy at a temperature of $T=20$ keV. In order to obtain an accurate result for the stopping length in this regime an adequate thermal average over the electron velocity distribution has to be performed, as Coulomb stopping is dominated by Coulomb collisions of slow electrons. After a lengthy calculation the author finds

$$\frac{dE_C}{dx} = \frac{4 (Z^2)}{m_e v} n_e \text{erf} \left(\frac{y}{v} \right) - 1 - \frac{T}{2m_e} + \frac{1}{2} v \frac{1}{v m_e} \frac{2}{p} = e^{y^2} \frac{y}{v} - 1 - \frac{T}{2m_e} + \frac{v^2}{8} + \frac{m_e v^4}{T} - \frac{T}{2m_e} \quad (D5)$$

for the Coulomb stopping which includes a thermal average over a Maxwell-Boltzmann distribution of electron (positron) velocities. Here $y = m_e v^2/2T$ such that for $y \gg 1$ one recovers the result Eq. (D1) where the velocities of all electrons are below that of the nucleus. The term p in Eq. (D5) denotes the logarithm in Eq. (D1). Note that in Eq. (D5) an expansion has been performed to lowest non-trivial order in the small parameters v and $T=m_e$, where both have been regarded to be of the same order.

b. Thomson scattering

Energetic protons may lose energy to the CMBR by Thomson scattering, a process which is particularly efficient at high CMBR temperature. Due to the large number of CMBR photons many scatterings are involved and the energy

loss of protons due to Thomson drag may also be treated as a continuous energy loss. Following Reno & Seckel [15] and own calculations one finds

$$\frac{dE_{Th}}{dx} = \frac{32}{9} \frac{2T^4}{15} \frac{2}{M_p^2} \frac{2}{v_p^2} v_p^2 Z^4; \quad (D 6)$$

for the energy loss per unit length where T and T are the structure constant and CM BR temperature, M_p the proton mass, v_p its gamma factor and velocity, and Z its electric charge. Note that Eq. (D 6) is applicable for protons of arbitrary relativity.

c. Magnetic moment scattering

Neutrons may lose energy due to scattering of electrons and positrons by virtue of their anomalous magnetic moment. This process is only important at higher temperature $T > 50$ keV due to the larger numbers of e . By aid of a calculation employing the relevant interaction amplitude one may find

$$\frac{dE_n}{dx} = \frac{3}{M_n^2} \frac{2^2 m_e^2}{n^2 v_n^2} n_e^2; \quad (D 7)$$

where $\gamma = 1.91$ is the anomalous magnetic dipole moment and all other notation is as before. Eq. (D 7) applies for non-relativistic as well as relativistic neutrons.

2. Electromagnetic Cascades Induced by γ -rays and Charged Particles

The injection of energetic electromagnetically interacting particles in the early Universe leads to a cascade on the CM BR with γ -rays pair-producing ($\gamma + \text{CM BR} \rightarrow e^+ + e^-$) and the produced electrons (positrons) inverse Compton scattering ($e^+ + \text{CM BR} \rightarrow e^+ + \gamma$) of the CM BR photons [50, 51, 52, 53, 54]. This cascade is very rapid due to the large number of CM BR photons. Only when γ -ray energies have fallen below that for pair production $E < m_e^2/E_{\text{CM BR}}$ interactions on protons and nuclei become important. The spectrum of these "breakout" photons below the pair production threshold depends essentially only on the total electromagnetically interacting energy E_0 injected above E_c . It has been found to be well approximated by [53, 54]

$$\frac{dN}{dE} = \begin{cases} \frac{8}{\gamma} K_0 \frac{E}{E_X}^{1.5} & \text{for } E < E_X \\ \frac{2}{\gamma} K_0 \frac{E}{E_X} & \text{for } E_c < E < E_X \end{cases}; \quad (D 8)$$

where $K_0 = E_0 = (E_X^2/2 + \ln(E_c/E_X))$ is a normalization constant such that the total energy in γ -rays below E_c equals the total energy E_0 injected. Following the analysis of Ref. [54] a value of $E_c = m_e^2/22T$ is employed in the present analysis with $E_X = 0.03E_c$ [51]. These values are very close to those ($E_c = m_e^2/23.6T$ and $E_X = 0.0264E_c$) advocated by Ref. [53]. Subsequent interactions of these "break-out" photons include photon-photon scattering ($\gamma + \text{CM BR} \rightarrow \gamma + \gamma$) mainly redistributing the energy of energetic γ -rays right below energy E_c , Bethe-Heitler pair production ($\gamma + p(^4\text{He}) \rightarrow p(^4\text{He}) + e^- + e^+$), Compton scattering ($\gamma + e^- \rightarrow \gamma + e^-$) of thermal electrons, with the produced energetic e^- inverse Compton scattering to generate further low-energy γ -rays, as well as nuclear photodisintegration. All these processes are included in the analysis and their detailed treatment is described below.

a. Bethe-Heitler pair production

The cross section for pair production by γ -rays of energy E scattering off protons and helium nuclei at rest is given by

$$\sigma_{BH} = \frac{3}{8} \frac{T_h}{T_h} \frac{28}{9} \ln \frac{2E}{m_e} - \frac{218}{27} Z^2; \quad (D 9)$$

where τ_{th} , m_e , and Z are Thomson cross section, fine structure constant, electron mass, and nuclear electric charge, respectively. The expression is valid in the regime $1 \ll E = m_e c^2 Z^{-1} \ll 1$. For energies in the range $2m_e < E < 4M\text{ eV}$ the cross section is roughly approximated as constant at the value of Eq. (D 9) at $E = 4M\text{ eV}$. The energy of the produced e^- (e^+) is approximated by a flat probability distribution within the range $[m_e; E - 2m_e]$ with the antiparticle e^+ (e^-) carrying the remainder of E .

b. Inverse Compton scattering

Electrons and protons produced during the dominant Bethe-Heitler process may upscatter CMBR photons to γ -ray energies by inverse Compton scattering. As these γ -rays may later photodisintegrate nuclei, a fairly accurate treatment of inverse Compton scattering is required. Here the exact inverse Compton scattering rate is unimportant since it is always large compared to the Hubble expansion. For the cumulative probability distribution that an e^- (e^+) of energy $E_e = m_e c^2$ upscatters a CMBR photon to energy $E = 4 \frac{2}{e} T x$, where T is CMBR temperature, one may find

$$P_{ic} = e^{-x} \left(1 + \frac{1}{4}x - \frac{1}{4}x^2 + (0;x) - \frac{1}{4}x^3 + \frac{3}{4}x \right); \quad (D 10)$$

with

$$(0;x) = \int_x^{Z^{-1}} dy e^{-y} = y \quad (D 11)$$

is an incomplete Gamma function. Note that for the evaluation of Eq. (D 10) the approximation that the e^- are ultrarelativistic, i.e. $e \gg 1$, and that the scattering process occurs in the Thomson regime, i.e. $12 \frac{e^2 T}{m_e} \ll 1$, have been made. These approximations are appropriate since only ultrarelativistic e^- may produce γ -rays by inverse Compton scattering on the CMBR which are energetic enough to photodisintegrate nuclei, and since e^- produced during Bethe-Heitler pair production are not energetic enough for the inverse Compton scattering to proceed in the Klein-Nishina limit. Furthermore for the derivation of Eq. (D 10) the Einstein-Bose occupation number $(e^{-E} - 1)^{-1}$ has been approximated by $(3)e^{-E}$ with $(3) = 1.2021$ such that the total number of CMBR photons remains the same. The approximation was required to find a closed form for P_{ic} . By comparison to an accurate numerical evaluation one finds that the approximation is typically good to within 3% - 10%. Lastly one finds for the average scattered CMBR photon energy a value of $hE_i = \frac{2}{e} hE_{CMBR}$ with $hE_{CMBR} = 2.701T$ the average CMBR photon energy.

c. Compton scattering

The cross section for γ -rays of energy E scattering off electrons at rest in the Klein-Nishina limit $E \gg m_e$ is given by [55]

$$e^{-\frac{3}{8} \frac{\tau_{th}}{!} \ln 2!} + \frac{1}{2} + O\left(\frac{\ln !}{!}\right) \quad ! \gg 1; \quad (D 12)$$

where $! = E/m_e$ and τ_{th} is the Thomson cross section. The cumulative probability distribution that the e^- scatters to energy $E^0 = E^c$ during the Compton scattering process may be derived by utilizing the results in Ref. [55] and is found as

$$P_c(E^0; E^0 - E^c) = \frac{\frac{1}{2}x^2 - \frac{\ln \frac{1}{x}}{x} + \ln 2!}{\frac{1}{2} + \ln 2!} + O(1=!) ; \quad (D 13)$$

where $x = E^c/E$ and the kinematic limits of x fall in the range 1 and $1=(1+2!) = 1=2!$. The scattered electrons may produce further γ -rays by inverse Compton scattering on the CMBR, an effect which is taken into account in the calculations.

d. - scattering

Following the analysis of Svensson & Zdziarski [51, 52] the total rate for scattering of a γ -ray of energy E on a blackbody of temperature T is given by

$$R = \frac{2^4 139}{3^6 5^4} \cdot 4m_e \cdot \frac{T}{m_e}^6 \cdot \frac{E}{m_e}^3 ; \quad (D 14)$$

Employing Eq.(3.9) of Ref. [52] one may compute the cumulative probability distribution for the energy of the scattered photon E^0 to be below E^c as

$$P_c(E^0; E^c) = \frac{10}{7} x^1 - x^2 - \frac{1}{2} x^3 + \frac{1}{5} x^4 ; \quad (D 15)$$

where $x = E^c/E = 1$. The energy of the scattered blackbody photon is given approximately by $E^0_{BB} = E - E^0$ in the limit $T \ll E$ and its effects are treated in the calculations as well.

3. Photodisintegration

Photodisintegration of the light-elements by γ -rays generated as a consequence of relic particle decays plays a particularly important role in the determination of BBN yields, as noted early on [12]. It is only effective at temperatures below $T < 6$ keV (cf. Fig. 5), since at higher temperatures γ -rays of sufficient energy $E \gtrsim 2$ MeV to photodisintegrate 2H , 7Li , and 7Be predominantly pair produce on the abundant CMBR photons (cf. App. D 2). Below this approximate cosmic temperature pair-production is kinematically forbidden such that photodisintegration becomes probable. The competing Bethe-Heitler pair production, Compton scattering and γ -scattering were described in the previous subsections.

The (lowest) photodisintegration thresholds for the various light nuclei synthesized during BBN 2H , 3H , 3He , 4He , 6Li , 7Li , and 7Be are given by 2.225 MeV, 6.257 MeV, 5.493 MeV, 19.814 MeV, 2.467 MeV, and 1.587 MeV, respectively. The present analysis utilizes photodisintegration data as parameterized by Ref. [19] with a few of these parameterizations changed to produce fits to the available reaction data. For original references the reader is referred to the references in Ref. [19].

In addition, the reactions 23–26, and 30–33, not considered in Ref. [19], have been included in the present analysis. Here the following parameterizations of reaction rate data [41, 56, 57] have been adopted:

Reaction 23 [41]:

$$(E) = 3.8 \text{ mb} Q_0^{2.3} (E - Q_0) = E^{3.3} + 2.1 \text{ mb} Q_1^{1.5} (E - Q_1) = E^{2.5} (E - Q_1) \quad (D 16)$$

with $Q_0 = 8.725$ MeV and $Q_1 = 23$ MeV and (x) the step function,

Reaction 24 [41, 56]:

$$(E) = 10.8 \text{ mb} Q^2 (E - Q)^{1.2} = E^{3.2} \quad (D 17)$$

with $Q = 9.98$ MeV, and

Reaction 25 [57]:

$$(E) = 1.44 \cdot 10^3 \text{ mb} Q^{2.0} (E - Q)^{2.4} = E^{22.4} \quad (D 18)$$

with $Q = 22.28$ MeV. Reaction 26 has been parameterized as reaction 25 but with $Q = 23.05$ MeV since no experimental data exists. Similarly, since no reaction rate data exists for the cross sections of reactions 30–33 they have been approximated by the data of their respective mirror reactions 23–26 but with binding energies appropriately replaced by, $Q = 7.08$ MeV, $Q = 10.68$ MeV, $Q = 22.17$ MeV, and $Q = 21.40$ MeV for reactions 30, 31, 32, and 33, respectively.

APPENDIX E: NON-THERMAL HADRONIC INTERACTIONS

1. Mesonic Induced Charge-exchange reactions

Injection of mesons in the form of metastable pions and kaons may induce the charge-exchange reactions 34-43 to convert protons to neutrons and vice versa [15]. As essentially each neutron is incorporated into a helium nuclei at $T = 80 \text{ keV}$, mesons may thus effect the ${}^4\text{He}$ abundance. Since more protons are converted to neutrons than vice versa, injection of mesons leads to an increase in the ${}^4\text{He}$ abundance. Mesonic charge-exchange reactions are particularly important at fairly high temperatures. At $T = 1 \text{ MeV}$, for example, a fraction 0.01 of all mesons induce charge exchange with the remainder decaying. In contrast, this fraction drops to 10^{-5} at $T = 100 \text{ keV}$. The present analysis follows the treatment of Ref. [15] and the reader is referred to this study for details.

The mesons may be due to a variety of processes. It is well known that the hadronic decay (or annihilation) results in a multitude of mesons. However, under certain circumstances even electromagnetic and weak-decays may yield mesons. This may be due to decays involving π^0 in the final state, which have a branching ratio to pions. Similarly injection of high-energy $E = 100 \text{ GeV}$ neutrinos at $T = 1 \text{ MeV}$ may pair-produce π^0 on the neutrino background. Pair-production of pions by γ -scattering on the CMBR [21] is unlikely as the Compton cross section is typically a factor 300 larger.

Production of mesons by electromagnetically or weakly interacting particles has not been included in the present study. In the case of hadronic decays their effect is subdominant, and in the case of electromagnetic and weak-decays the analysis is model-dependent on the decay products.

2. Nucleon-Antinucleon Annihilations

Hadronic decays lead to the production of nucleons and anti-nucleons. It is assumed here that the total baryon number is conserved during the decay. At higher temperatures ($T > 90 \text{ keV}$ for n and n and $T > 20 \text{ keV}$ for p and p) they thermalize by electromagnetic energy losses (cf. App. D.1) with antinucleons annihilating at rest thereafter. The combination of injection of nucleons (with a predefined $n=p$ -ratio, typically close to one) and annihilation of antinucleons on the pre-existing nucleons may lead to an increase of the neutron-to-proton ratio and the ${}^4\text{He}$ abundance resulting from BBN [15]. Antinucleons mostly annihilate on protons due to the small thermal $n=p$ -ratio and due to Coulomb enhancement of the pp annihilation cross section. The annihilated protons are replaced by the injected nucleons which typically come in a ratio $n=p=1$ thus yielding an effective increase of the $n=p$ -ratio. Given a typical injected meson-to-(anti-)baryon ratio of 20 in hadronic decays the effects of nucleon anti-nucleon injection are far more important than those of mesonic charge exchange reactions. This holds particularly true at lower temperatures $T < 300 \text{ keV}$. The present study uses the reaction rate data as given in Ref. [15].

When electromagnetic stopping becomes dominant at lower temperatures thermalization of energetic nucleons occurs partially due to nucleon-nucleon scattering and nuclear spallation (cf. App. E.3, E.4, E.5). Antinucleons, on the other hand, never thermalize but rather annihilate during one of their first interactions with thermal protons or helium nuclei. As an energetic nucleon has of the order of 20 N_{sc} scattering events before dropping below the ${}^4\text{He}$ spallation threshold its probability to inflict a ${}^4\text{He}$ spallation event is factor 10 larger than that of an antinucleon. It has been therefore approximated that antinucleons do never spall ${}^4\text{He}$, leading to an about 10% underestimate in ${}^2\text{H}$, ${}^3\text{H}$, and ${}^3\text{He}$ production due to particle decay.

3. Elastic N-N scattering

Elastic nucleon-nucleon scattering and nucleon- ${}^4\text{He}$ scattering of energetic neutrons and protons on the thermal protons and ${}^4\text{He}$ is important in the nucleon thermalization process in particular at lower temperature ($T < 90 \text{ keV}$ for n 's and $T < 20 \text{ keV}$ for p 's) and when the nucleons are not too energetic, i.e. $E < 1 \text{ GeV}$. This may be seen in Fig. 1. In contrast, very energetic nucleons, $E = 1 \text{ GeV}$, are stopped at lower temperatures mostly by inelastic scatterings of protons and ${}^4\text{He}$ (cf. App. E.4, and E.5) and at higher temperatures either by Thomson scattering on CMBR photons in the case of protons (cf. App. D.1.b) or magnetic moment scatterings on thermal ${}^4\text{He}$ in the case of neutrons (cf. App. D.1.c). Elastic scatterings on protons also produce secondary energetic protons which are taken into account in the present study.

For the elastic $p-p$, $n-p$, $p-{}^4\text{He}$, and $n-{}^4\text{He}$ scattering cross sections we take the data as compiled by Ref. [44]. This compilation compares well with that given in the more recent compilation given in Ref. [58]. It is noted here that

due to approximate isospin invariance the $p-^4He$ and $n-^4He$ cross sections are almost equal. To calculate the energy loss in $p-p$ and $n-p$ scattering events, an against nuclear data tested algorithm presented in Ref. [45] is used. Each scattering event is treated by a Monte Carlo. This algorithm predicts an almost uniform probability distribution for fractional energy loss $E_k = E_k$ for < 250 MeV protons progressing smoothly towards a bimodal probability distribution (either forward scattering, i.e. $E_k = E_k = 0$ or backward scattering, i.e. $E_k = E_k = 1$) when the p kinetic energy is increased towards 2 GeV. Neutron-proton scattering follows a similar though less well-defined trend. For kinetic energies $E_k > 2$ GeV the probability distributions of 2 GeV nucleons are utilized.

Nucleon- 4He scattering follows a very different pattern with 4He recoil energies to high probability very small. Given data by Ref. [59] the typical 4He recoil energy is approximated at 5 MeV in each event. It has been verified that a change in this recoil energy has negligible effect on the BBN yields. For a more detailed discussion on the 4He recoil energies which play a role in $^4He-^4He$ fusion reactions 87 and 88 the reader is referred to App. E.6.

4. Inelastic $N \rightarrow N$ scattering

For nucleon-nucleon scattering with nucleon kinetic energies in the GeV range scattering processes are mostly inelastic accompanied by the production of pions. Treating these processes properly is important not only for a determination of the typical nucleon energy loss, but also because scattering processes may easily convert protons to neutrons and vice versa. In fact, due to a large asymmetry in the cross sections the conversion of energetic protons to neutrons occurs more often than the inverse of this process. This has implication for spallation processes, increasing 2H , 3H , 3He , and 6Li yields, as neutrons are stopped by scattering off protons and 4He for temperatures $T < 90$ keV, whereas $E_p < 1$ GeV protons mostly lose their energy via Coulomb stopping. This study uses the inelastic $N \rightarrow N$ cross sections reactions 52 – 73 in Table 1 as compiled by Ref. [46], where some of the proposed fitting functions had to be modified by the author to correctly account for the data. Concerning the total average energy loss f into pion mass and kinetic energy in inelastic scatterings experimental data by Ref. [69] at $E_p = 790$ MeV and a simulation with Pythia at $E_p = 53$ GeV has been fitted logarithmically to obtain $f = 0.2 + 0.08 \ln(E = 0.8 \text{ GeV})$. The remainder of the energy has been split in proportions (0.15, 0.85) between the outgoing nucleons roughly equal to the average energy split for energetic elastic collisions. For the nucleon energy loss in the inelastic spallation processes discussed in App. E.5 it has been assumed that the outgoing nucleons are missing the binding energy necessary for the spallation process, and the remaining energy is shared between primary and secondary nucleon in proportion (0.75, 0.25). This corresponds to the average values for elastic $N \rightarrow N$ scattering in the several hundred of MeV range.

5. Nuclear spallation

A side from 4He photodisintegration which is operative only at lower cosmological temperatures $T < 3$ keV 4He spallation reactions at temperatures $T < 90$ keV induced by energetic nucleons are the main source of additional 2H , 3H , 3He , as well as 6Li (through nonthermal fusion reactions induced by energetic 3-nuclei, cf. App. E.6) in BBN with decaying particles. It is therefore important to employ accurate reaction cross section data. The 4He -spallation reactions 74 – 83 in Table 1 have been included in the analysis. Experimental data on these reactions has been obtained at nucleon energies $E = 28$ MeV [60], 53 MeV [61], 90 MeV [62], 220 MeV [63], 300 MeV [64], 620 MeV [65], 1.42 GeV [66], and 2.61 GeV [66], respectively, and has been interpolated in between. This data and the interpolation is shown in Fig. 11. The data also includes the possible production of additional pions in the spallation process. Note that 4He -spallation data induced by either neutrons or protons has been included on equal basis in the compilation. Here reactions induced by neutrons, such as $^4He(n; np)^3H$, have been associated with their corresponding mirror reactions induced by protons, i.e. $^4He(p; np)^3He$. This is theoretically and experimentally justified due to approximate isospin invariance, as long as Coulomb effects are negligible, in particular, for nucleon energies larger than a few MeV. For the energies of nucleons and nuclei after the spallation the reader is referred to App. E.4 and E.6. The spallation of energetic freshly synthesized 6Li reaction 84 has also been included [67] but plays only a minor role for the results.

6. Non-Thermal Fusion Reactions

Non-thermal fusion reactions are particularly important for the formation of 6Li which during thermal BBN is produced only in very small amounts. When relic particles decay during or after BBN 6Li is therefore the first element which becomes significantly perturbed compared to its SBBN abundance. This has been shown first in the case of

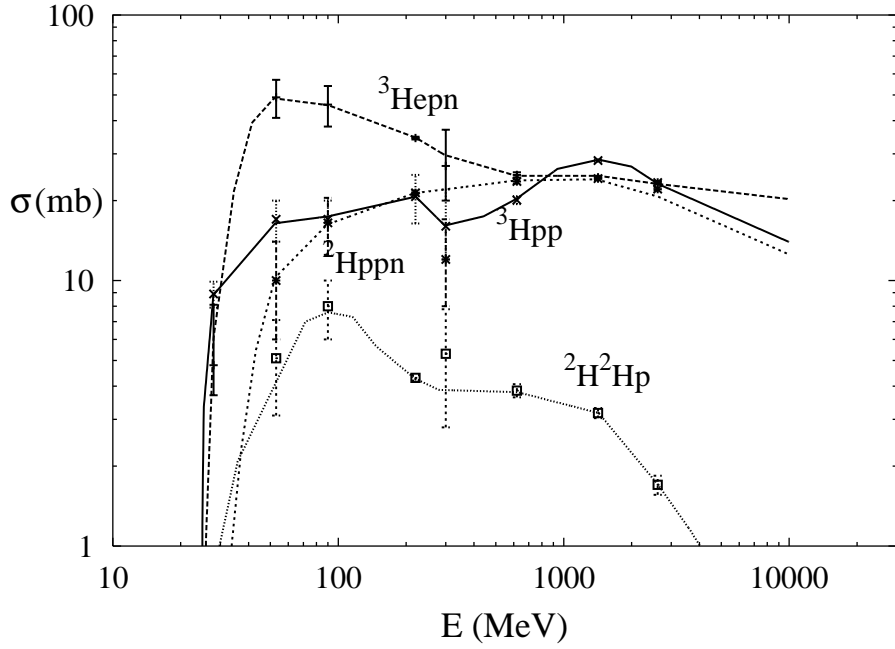


FIG. 11: Compilation of the available ^4He spallation data as a function of nucleon kinetic energy (with ^4He at rest) for the spallation reactions 74, 75, 76, and 78. The lines joining independent data points (74 – solid; 75 – long-dashed, 76 – short-dashed, 78 – dotted) represent the τ used in the present analysis. Refer to the text for references.

hadronic decays in Ref. [14] and later in the case of electromagnetic decays in Ref. [17]. The most efficient reaction sequence is initiated by either the spallation $^4\text{He}(N, \gamma)$ or photodisintegration $^4\text{He}(e^-, e^-)$ to produce energetic ^3H and ^3He nuclei. These later may then fuse on ambient ^4He -nuclei to form ^6Li via $^3\text{H}(^4\text{He}; n)^6\text{Li}$ and $^3\text{He}(^4\text{He}; p)^6\text{Li}$. If only a small fraction 10^{-4} (cf. Fig. 2) of these energetic 3-nuclei fuse an observationally important ^6Li abundance may result. Energetic 3-nuclei in the tens of MeV range are essentially all stopped by Coulomb interactions. Since this process is less efficient at higher energy (i.e. $(1=E_3)dE_3=dx/E_3^2$; cf. App. D.1 a) and since the fusion cross section does not drastically fall with energy the formation of ^6Li is very sensitive towards the high-energy tail of produced 3-nuclei. It will be seen that the lack of knowledge of this tail actually introduces some uncertainty in the ^6Li yield.

In this paper the $^3\text{H}(^4\text{He}; n)^6\text{Li}$ and $^3\text{He}(^4\text{He}; p)^6\text{Li}$ cross sections as determined with the aid of reverse reaction rate data by Ref. [68] and Ref. [19], respectively, have been adopted. Here the first reaction has a threshold in the ^4He rest frame of $E_{th} = 8.39\text{ MeV}$, whereas the second reaction has $E_{th} = 7.05\text{ MeV}$. Cross sections for the spallation and photodisintegration reactions are taken as described in App. E 5 and App. D 3, respectively. Concerning the "recoil" energy distributions of the 3-nuclei in the case of photodisintegration it is given by $E_3 = (E - E_{th}^{^4\text{He}})m_N/(m_N + m_3)$ for ^3H nuclei, whereas for spallation one has to resort to experimental data. Data has been published for the $^4\text{He}(n; np)^3\text{H}$ reaction [62] at $E_n = 90\text{ MeV}$ in the ^4He rest frame and more recently for the $^4\text{He}(p; pp)^3\text{H}$ and $^4\text{He}(p; np)^3\text{He}$ reactions [70] at $E_p = 220\text{ MeV}$. Data at higher energies exists as well [71] which lies above the threshold of pion production during the spallation process. In general, the energy distributions of 3-nuclei seem almost independent of incident nucleon energy though care has to be taken in the comparison since sometimes only partial (quasi-free-scattering) distributions are shown (as in the case of Ref. [71]). In this study the complete distributions as given in Ref. [70] are utilized (in binned form) for both the $^4\text{He}(p, \gamma)$ reactions and their $^4\text{He}(n, \gamma)$ corresponding mirror reactions. The utilization of reaction rate data of the corresponding mirror reactions seems not only theoretically justified [44, 72] but also when experimental data of Ref. [62] and Ref. [70] are directly compared.

Some uncertainty in the ^6Li yield results from an inaccurate determination of the few percent high-energy tail in the 3-nuclei energy distribution function. The highest energy events are particularly difficult to detect in bubble chamber experiments [72], such that the distribution of Ref. [70] only extends towards $E_3 = 90\text{ MeV}$. In Ref. [62] a fraction of about 2% of all spallation reactions seem to result in ^3H nuclei at the kinematically highest allowed energy. This corresponds to backward scattering and such peaks in the distribution functions are also observed in $^4\text{He}-^4\text{He}$ elastic scatterings [73]. If the four-event backward scattering peak as observed in Ref. [62] is real, rather than a fluctuation or measurement error, resulting ^6Li yields may increase by some tens of per cents due to these high-energy 3-nuclei.

(cf. Fig. 2). However, on conservative grounds this study neglects ^6Li production due to the very highest energy 3-nuclei.

Energetic 3-nuclei may also be produced by $^4\text{He}(n; ^2\text{H})^3\text{H}$ and its mirror reaction. For the energy distributions of this subdominant 3-nuclei channel reaction data of the compilation/derivation in Refs. [44, 74] at proton kinetic energies of 55 MeV, 85 MeV, and 156 MeV, respectively, have been interpolated. Fusion reactions such as $^2\text{H}(;)^6\text{Li}$, $^3\text{H}(;)^7\text{Li}$, and $^3\text{He}(;)^7\text{Be}$ have not been considered as cross sections involving the emission of a photon are typically only in the nb to b range. The $\text{N}(\text{N} ; ^0\text{s})^2\text{H}$ reaction, on the other hand is treated as discussed in App. E 4.

Note that in a narrow temperature interval around $T = 3 - 20$ keV Coulomb stopping of not too energetic $E_{10} = 30$ MeV 3-nuclei loses its efficiency (cf. App. D 1a) due to the nuclei velocity falling below a typical electron thermal velocity. In this regime of efficient ^6Li synthesis other processes reactions 89 – 91 which contribute to the thermalization of 3-nuclei may become of some limited importance. They have been included in the calculation by taking data from Ref. [75]. At very low temperatures $T < 1$ eV energetic ^3H stopping times may become longer than the ^3H decay time. It is therefore possible that ^3H decays to ^3He before it falls below the ^6Li fusion threshold and this effect has been taken into account.

Fusion reaction between energetic ^4He (produced by N^4He elastic scatterings) and thermal ^4He -nuclei may, in principle, also lead to the synthesis of ^6Li , as well as ^7Li . In practice, however, this process is subdominant and has therefore not been included. The threshold energies for $^4\text{He}(; p)^7\text{Li}$ and $^4\text{He}(; pn)^6\text{Li}$ are 37.8 MeV and 49.2 MeV, respectively. These are much larger than those for the fusion of 3-nuclei on ^4He . Given the data in Ref. [59] the distribution function for recoil energies of ^4He -nuclei in N^4He elastic scattering may be approximated by an exponential distribution $dP = dE_4 \propto a \exp(-bE_4)$ with $a = 225 \text{ mb/GeV}$ and $b = 65 \text{ GeV}^{-1}$, independent of nucleon kinetic energy. The total cross section for producing $E_4 > 50$ MeV recoil ^4He in N^4He scatterings is thus in the

0.1 mb range. Note that $E_4 > 50$ MeV has been chosen as only for such energies the $^4\text{He}^4\text{He}$ fusion cross section becomes appreciable (100 mb [76]). The cross section of 0.1 mb for the production of ^4He nuclei energetic enough to produce ^6Li by fusion has to be compared to the typical total cross sections for $^4\text{He}(\text{N} ; \dots)^3\text{H}$, etc. of 30 mb times the fraction 0.3 of 3-nuclei energetic enough to fuse to ^6Li . This yields 10 mb compared to 0.1 mb. Nevertheless, ^6Li fusion via ^4He -nuclei is enhanced due to a less efficient Coulomb stopping at 50 MeV versus the canonical 10 MeV for 3-nuclei, resulting in an enhancement factor of $(50/10)^2 = 4$. Here the 4 in the denominator comes from the factor two higher charge of ^4He nuclei compared to ^3H nuclei. Altogether it is found that energetic ^4He contributes only of the order 6% to the total ^6Li abundance. This is also not changed by the existence of a sharp backward scattering peak in N^4He scattering [73] which, similarly to the possible existence of a backward peak in the 3-nuclei distribution (see above) may increase the ^6Li synthesis due to energetic ^4He by a factor 1.2.

APPENDIX F: THERMAL NUCLEAR REACTIONS

Thermal nuclear reactions are treated by the Kawano code updated by the NACRE [77] reaction compilation. For the neutron life time the value $n = 885.7$ sec is used as quoted as the ‘world’ average in the Particle Data Booklet. For the fractional contribution of baryons to the critical density the central value as determined by three years of WMAP observations [2] $bh^2 = 0.02233^{+0.072}_{-0.091}$ is applied. Given the conversion $bh^2 = 3.65 \cdot 10^7$ this corresponds to a baryon-to-photon ratio of $n_b/n = 6.12 \cdot 10^{10}$. With these input values the abundances within a SBBN scenario are found at $^2\text{H}/\text{H} = 2.68 \cdot 10^{-5}$, $^3\text{He}/^2\text{H} = 0.38$ ($^3\text{He}/\text{H} = 1.04 \cdot 10^{-5}$) $Y_p = 0.248$, and $^7\text{Li}/\text{H} = 4.34 \cdot 10^{-10}$, respectively. The ^6Li abundance in a SBBN scenario is negligible compared to the observationally inferred value of ^6Li in low-metallicity stars.

[1] R. A. Malaney and G. J. Mathews, Phys. Rept. 229, 145 (1993); S. Sarkar, Rept. Prog. Phys. 59, 1493 (1996); K. Jedamzik, astro-ph/9805156; H. Kurki-Suonio, astro-ph/0002071.

[2] D. N. Spergel et al., astro-ph/0603449.

[3] M. H. Pinsonneault, T. P. Walker, G. Steigman and V. K. Narayanan, Astrophys. J. 527, 180 (2002).

[4] O. Rieckhard, G. Michaud and J. Richer, Astrophys. J. 619, 538 (2005).

[5] M. Salaris and A. Weiss, Astrophys. J. 376, 955 (2001);

[6] S. Theado and S. Vauclair, Astrophys. J. 375, 70 (2001).

[7] L. Piau, T. C. Beers, D. S. Balsara, T. Sivarani, J. W. Tumaran and J. W. Ferguson, astro-ph/0603553.

[8] K. Jedamzik, Phys. Rev. D 70, 063524 (2004).

[9] K. Jedamzik, K. Y. Choi, L. Roszkowski and R. Ruiz de Austri, hep-ph/0512044.

[10] S. Weinberg, Phys. Rev. Lett. 48, 1303 (1982); H. Pagels and J. R. Primack, Phys. Rev. Lett. 48, 223 (1982); M. Y. Khlopov and A. D. Linde, Phys. Lett. B 138, 265 (1984).

[11] F. Balestra et al., Lett. Nuovo Cim. 41, 223 (1984).

[12] D. Lindley, Astrophys. J. 294, 1 (1985).

[13] J. Ellis, D. Nanopoulos, and S. Sarkar, Nucl. Phys. B 259, 175 (1985); R. Juszkiewicz, J. Silk and A. Stebbins, Phys. Lett. B 158, 463 (1985); A. udouze, D. Lindley and J. Silk, Astrophys. J. 293, L53 (1985); D. Lindley, Phys. Lett. B 171, 235 (1986); M. Kawasaki and K. Sato, Phys. Lett. B 189, 23 (1987); R. J. Scherrer and M. S. Turner, Astrophys. J. 331, 19 (1988); Y. L. Levitan, I. M. Sobol, M. Y. Khlopov and V. M. Chechetkin, Sov. J. Nucl. Phys. 47, 109 (1988).

[14] S. Dimopoulos, R. Esmaeilzadeh, L. J. Hall and G. D. Starkman, Astrophys. J. 330, 545 (1988); S. Dimopoulos, R. Esmaeilzadeh, L. J. Hall and G. D. Starkman, Nucl. Phys. B 311, 699 (1989).

[15] M. H. Reno and D. Seckel, Phys. Rev. D 37, 3441 (1988).

[16] J. R. Ellis, G. B. Gelmini, J. L. Lopez, D. V. Nanopoulos and S. Sarkar, Nucl. Phys. B 373, 399 (1992); M. Kawasaki and T. M. Oroi, Prog. Theor. Phys. 93, 879 (1995); J. Protheroe, T. Stanev and V. S. Berezinsky, Phys. Rev. D 51, 4134 (1995); M. Yu. Khlopov, Yu. L. Levitan, E. V. Sedelnikov and I. M. Sobol, Phys. Atom. Nucl. 57, 1393 (1994); E. V. Sedelnikov, S. S. Filippov and M. Y. Khlopov, Phys. Atom. Nucl. 58, 235 (1995); E. Holtmann, M. Kawasaki, K. Kohri and T. M. Oroi, Phys. Rev. D 60, 023506 (1999).

[17] K. Jedamzik, Phys. Rev. Lett. 84, 3248 (2000).

[18] M. Kawasaki, K. Kohri and T. M. Oroi, Phys. Rev. D 63, 103502 (2001); K. Kohri, Phys. Rev. D 64, 043515 (2001).

[19] R. H. Cyburt, J. R. Ellis, B. D. Fields and K. A. Olive, Phys. Rev. D 67, 103521 (2003).

[20] M. Kawasaki, K. Kohri and T. M. Oroi, Phys. Lett. B 625, 7 (2005).

[21] M. Kawasaki, K. Kohri and T. M. Oroi, Phys. Rev. D 71, 083502 (2005).

[22] K. Jedamzik, Phys. Rev. D 70, 083510 (2004).

[23] D. G. Cerdeno, K. Y. Choi, K. Jedamzik, L. Roszkowski and R. Ruiz de Austri, hep-ph/0509275.

[24] M. Asplund, D. L. Lambert, P. E. Nissen, F. Primas and V. V. Smirnov, astro-ph/0510636.

[25] G. Steigman, Int. J. Mod. Phys. E 15, 1 (2006).

[26] B. Fields and S. Sarkar, astro-ph/0601514.

[27] Y. I. Izotov and T. X. Thuan, Astophys. J. 602, 200 (2004).

[28] V. Luridiana, A. Peimbert, M. Peimbert and M. Cervino, Astophys. J. 592, 846 (2003).

[29] K. A. Olive and E. D. Skillman, Astophys. J. 617, 29 (2004).

[30] J. M. O'Meara, D. Tytler, D. Kirkman, N. Suzuki, J. X. Prochaska, D. Lubin and A. M. Wolfe, Astophys. J. 552, 718 (2001); M. Pettini and D. V. Bowen, Astophys. J. 560, 41 (2001); D. Kirkman, D. Tytler, N. Suzuki, J. M. O'Meara and D. Lubin, Astophys. J. Suppl. 149, 1 (2003); N. H. M. Crighton, J. K. Webb, A. Ortiz-Gill and A. Fernandez-Soto, Mon. Not. Roy. Astron. Soc. 355, 1042 (2004).

[31] G. Sigl, K. Jedamzik, D. N. Schramm and V. S. Berezinsky, Phys. Rev. D 52, 6682 (1995).

[32] G. G. Beckler and J. G. Eiss, Light Elements and their evolution, IAUS symposia 198, 224 (2000).

[33] P. Bonifacio and P. Molaro, Mon. Not. Roy. Astron. Soc. 285, 847 (1997).

[34] S. G. Ryan, J. E. Norris and T. C. Beers, Astophys. J. 523, 654 (1999).

[35] V. V. Smirnov, D. L. Lambert, and P. E. Nissen, Astophys. J. 408, 262 (1993); 506, 405 (1998); R. Cayrel, M. Spite, F. Spite, E. Vangioni-Flam, M. Casse, and J. A. udouze, Astron. & Astophys. 343, 923 (1999); P. E. Nissen, M. Asplund, V. H. ill, and S. D. O'dorico, Astron. & Astophys. 357, L49 (2000).

[36] Cross section approximated by the parametrization given in Ref. ([19]) after comparison with published data in the Experimental Nuclear Reaction Data Base (EXFOR). For the original references the reader is referred to the EXFOR database and Ref. ([19]).

[37] Prefactor in the parametrizations of this reaction in Ref. ([19]) changed from 17.1 mb to 20.7 mb to account for EXFOR data.

[38] Prefactor in Ref. ([19]) changed from 104 mb to 143 mb to account for EXFOR data.

[39] The parametrization as given in Ref. ([19]) is adopted. Nevertheless, when reverse reaction rate data from NACRE [40] is used to evaluate the cross section the parametrization leads to a factor 2–3 overestimate of the cross section. In contrast, when direct reaction data assembled by Ref. [41] is used the parametrization leads to a factor 2–3 underestimate of the cross section. Other direct reaction rate data, such as of Ref. [42] also does not lead to a favorable comparison. It is concluded that the adopted $^7\text{Li}(; ^3\text{H})^4\text{He}$ cross section has large uncertainties. Since constraints from ^7Li are rather weak this has only little impact on the presented constraints.

[40] C. Angulo et al., Nucl. Phys. A 656, 3 (1999).

[41] V. V. Varlamov et al., BCD FE/L12, Fotojad.Danny - Photodisintegration of Lithium, Suppl., Moscow (1986).

[42] G. M. Gribus et al., Can. J. Phys. 39, 1397 (1961).

[43] The parametrization of Ref. ([19]) is adopted with nevertheless negative values of which occur at larger E in this parametrization set to zero. Direct reaction data for this reaction does not exist. As in the case of the reaction $^7\text{Li}(; ^3\text{H})^4\text{He}$ an evaluation of the cross section by the author utilising reverse reaction rate data from Ref. [40] indicates a possible overestimate of the cross section as parametrized in Ref. ([19]). Nevertheless, as constraints from other light elements are more stringent, this possible overestimate has only negligible influence on the conclusions.

[44] J. P. Meyer, Astron. & Astophys. Suppl. 7, 417 (1972).

[45] R. A. Arndt, I. I. Strakovsky and R. L. Workman, Int. J. Mod. Phys. A 18, 449 (2003); Fortran program SAID for the calculation of nucleon-nucleon amplitudes, <http://gwadac.phys.gwu.edu>, with courtesy provided by Dick Arndt.

[46] J. Bystricky, P. La France, F. Lehar, F. Perrot, T. Siemianczuk, & P. Winternitz, Journal de Physique 48, 1901 (1987).

[47] A n own t to the date has been used since the t as proposed by Ref. [46] is not adequate.

[48] J. D . Jackson, in *C lassical E lectrodynam ics*, John W iley and Sons Inc. 1999.

[49] R . G ould, in *H igh E nergy Phenom ena in Physics*, University of California, San D iego, lecture notes.

[50] F .A .A haronian, V .G .K irillov-U gryum ov, and V .V .V ardanian, *A strophys. Space Sci.* 115, 201 (1985).

[51] A .A .Zdziarski and R .Svensson, *A strophys. J.* 344, (1989), 551.

[52] R .Svensson and A .A .Zdziarski, *A strophys. J.* 349, (1990), 415.

[53] R .J .P rotheroe, T .Stanev, and V .S .Berezinsky, *Phys. Rev. D* 51, 4134 (1995)

[54] M .K awasaki and T .M .oroi, *A strophys. J.* 452, 506 (1995).

[55] C .Itzykson and J.-P .Zuber, in *Q uantum F ield T heory*, McG raw -H ill Book C om pany 1980.

[56] Yu M .Volkov et al., *J,ZET* ,42,108 (1962); V .P .Denisov et al., *J,YF* ,5, 490 (1967).

[57] E A .K otikov et al., *J,YF* ,46,1009 (1987).

[58] The Review of P article Physics, S .E idelm ann et al., *Phys. Lett. B* 592, 1 (2004); \http://pdg.lblgov/".

[59] L .G .Votta et al., *Phys. Rev. C* , 10, 520 (1974); V .C oparat et al., *Phys. Rev. C* 12, 251 (1975); R .K lem et al., *Phys. Lett. B* 70, 155 (1977); V .V .G lagolev et al., *Phys. Rev. C* 18, 1382 (1978).

[60] A .F .W ickersham , *Phys. Rev.* 107, 1050 (1957).

[61] D .J .C airms et al., *Nucl. Phys.* 60, 369 (1964).

[62] P .E .T annenwald, *Phys. Rev.* 89, 508 (1953).

[63] S .K .A bdullin et al., *Nucl. Phys. A* 569, 753 (1994).

[64] W .H .Innes, U niv. of C alifornia Radiaztion Laboratory Report U C R L-8040 .

[65] A .V .B linov et al., *Phys. of Atom ic N uclei*, 64, 907 (2001).

[66] V .V .G lagolev et al., *Zeit. Phys.C* 60, 421 (1993).

[67] A .J .E lwyn et al., *Phys. Rev. C* 20, 1984 (1979).

[68] E .S ihvola, *Phys. Rev. D* 63, 103001 (2001).

[69] W .T hom as et al., *Phys. Rev. D* 24, 1736 (1981).

[70] A .V .B linov et al., *Phys. of Atom ic N uclei* 58, 1713 (1995).

[71] V .V .G lagolev et al., *Phys. Rev. C* 18, 1382 (1978); A .D imer et al., *Eur. Phys. J. A* 8, 493 (2000).

[72] M arina C hadeyeva, private communication.

[73] J .Berger et al., *Phys. Rev. Lett.* 41, 152 (1978).

[74] L .G .Votta et al., *Phys. Rev. C* 10, 520 (1974).

[75] B .H aesner et al., *Phys. Rev. C* 28, 995 (1983).

[76] B .G .G lagola et al., *Phys. Rev. Lett.* 41, 1698 (1978); D .J .M eroer et al., *Phys. Rev. C* 63 065805 (2001).

[77] C .A ngulo et al., *Nucl. Phys. A* 656, 3 (1999).